



## City Research Online

### City, University of London Institutional Repository

---

**Citation:** Wang, Y., Cai, G., Li, Y., Waldmann, D., Si Larbi, A. & Tsavdaridis, K. D. (2019). Behavior of Circular Fiber-Reinforced Polymer-Steel-Confined Concrete Columns Subjected to Reversed Cyclic Loads: Experimental Studies and Finite-Element Analysis. *Journal of Structural Engineering*, 145(9), 04019085. doi: 10.1061/(asce)st.1943-541x.0002373

This is the accepted version of the paper.

This version of the publication may differ from the final published version.

---

**Permanent repository link:** <https://openaccess.city.ac.uk/id/eprint/26993/>

**Link to published version:** [https://doi.org/10.1061/\(asce\)st.1943-541x.0002373](https://doi.org/10.1061/(asce)st.1943-541x.0002373)

**Copyright:** City Research Online aims to make research outputs of City, University of London available to a wider audience. Copyright and Moral Rights remain with the author(s) and/or copyright holders. URLs from City Research Online may be freely distributed and linked to.

**Reuse:** Copies of full items can be used for personal research or study, educational, or not-for-profit purposes without prior permission or charge. Provided that the authors, title and full bibliographic details are credited, a hyperlink and/or URL is given for the original metadata page and the content is not changed in any way.

---

City Research Online:

<http://openaccess.city.ac.uk/>

[publications@city.ac.uk](mailto:publications@city.ac.uk)

---



City Research Online

## City, University of London Institutional Repository

---

**Citation:** Wang, Y, Cai, G, Li, Y, Waldmann, D, Si Larbi, A and Tsavdaridis, KD ORCID: 0000-0001-8349-3979 (2019). Behavior of Circular Fiber-Reinforced Polymer-Steel-Confining Concrete Columns Subjected to Reversed Cyclic Loads: Experimental Studies and Finite-Element Analysis. *Journal of Structural Engineering (United States)*, 145(9), doi: 10.1061/(ASCE)ST.1943-541X.0002373

This is the draft version of the paper.

This version of the publication may differ from the final published version.

---

**Permanent repository link:** <https://openaccess.city.ac.uk/id/eprint/26993/>

**Link to published version:** [http://dx.doi.org/10.1061/\(ASCE\)ST.1943-541X.0002373](http://dx.doi.org/10.1061/(ASCE)ST.1943-541X.0002373)

**Copyright:** City Research Online aims to make research outputs of City, University of London available to a wider audience. Copyright and Moral Rights remain with the author(s) and/or copyright holders. URLs from City Research Online may be freely distributed and linked to.

**Reuse:** Copies of full items can be used for personal research or study, educational, or not-for-profit purposes without prior permission or charge. Provided that the authors, title and full bibliographic details are credited, a hyperlink and/or URL is given for the original metadata page and the content is not changed in any way.

---

City Research Online:

<http://openaccess.city.ac.uk/>

[publications@city.ac.uk](mailto:publications@city.ac.uk)

---



UNIVERSITY OF LEEDS

This is a repository copy of *Behavior of Circular Fiber-Reinforced Polymer–Steel-Confined Concrete Columns Subjected to Reversed Cyclic Loads: Experimental Studies and Finite-Element Analysis*.

White Rose Research Online URL for this paper:  
<http://eprints.whiterose.ac.uk/143846/>

Version: Accepted Version

---

**Article:**

Wang, Y, Cai, G, Li, Y et al. (3 more authors) (2019) Behavior of Circular Fiber-Reinforced Polymer–Steel-Confined Concrete Columns Subjected to Reversed Cyclic Loads: Experimental Studies and Finite-Element Analysis. *Journal of Structural Engineering*, 145 (9). 04019085. ISSN 0733-9445

[https://doi.org/10.1061/\(ASCE\)ST.1943-541X.0002373](https://doi.org/10.1061/(ASCE)ST.1943-541X.0002373)

---

©2019 American Society of Civil Engineers. This is an author produced version of a paper published in *Journal of Structural Engineering*. Uploaded in accordance with the publisher's self-archiving policy.

**Reuse**

Items deposited in White Rose Research Online are protected by copyright, with all rights reserved unless indicated otherwise. They may be downloaded and/or printed for private study, or other acts as permitted by national copyright laws. The publisher or other rights holders may allow further reproduction and re-use of the full text version. This is indicated by the licence information on the White Rose Research Online record for the item.

**Takedown**

If you consider content in White Rose Research Online to be in breach of UK law, please notify us by emailing [eprints@whiterose.ac.uk](mailto:eprints@whiterose.ac.uk) including the URL of the record and the reason for the withdrawal request.



[eprints@whiterose.ac.uk](mailto:eprints@whiterose.ac.uk)  
<https://eprints.whiterose.ac.uk/>

# Behaviour of Circular FRP-Steel Confined Concrete Columns Subjected to Reversed Cyclic Loads: Experimental Studies and FE Analysis

Yanlei Wang<sup>1</sup>, Gaochuang Cai<sup>2\*</sup>, Yunyu Li<sup>3</sup>, Danièle Waldmann<sup>4</sup>, Amir Si Larbi<sup>5</sup>,

Konstantinos Daniel Tsavdaridis<sup>6</sup>

## Abstract

This paper studies experimentally the behaviour of circular FRP-steel confined concrete columns subjected to reversed cyclic loads. The influence of main structural factors on the cyclic behaviour of the columns is discussed. Test results show the outstanding seismic performance of FRP-steel confined reinforced concrete (RC) and steel-reinforced concrete (SRC) columns. The lateral confinement effectiveness of GFRP tube and GFRP-steel tube was verified and a simplified OpenSees-based finite element method (FEM) model was developed to simulate the experimental results of the test columns. Based on the proposed FEM model, a parametric analysis was conducted for investigating the effects of main factors on the reversed cyclic behaviour of GFRP-steel confined RC columns. Based on the test and numerical analyses, the study discussed the influence of variables such as the lateral confinement on the plastic hinge region (PHR) height and peak drift ratio of the columns under reversed cyclic loads. Results indicate that the lateral confinement significantly affects the PHR height of the circular confined RC columns. Based on the analyses of the data from this study and literature, a simple model was suggested to predict the peak drift ratio of the confined RC columns.

---

<sup>1</sup> Associate professor, State Key Laboratory of Coastal and Offshore Engineering, School of Civil Engineering, Dalian University of technology, Dalian 116024, China.

<sup>2</sup> Invited professor, Univ Lyon, Ecole Nationale d'Ingénieurs de Saint-Etienne (ENISE), Laboratoire de Tribologie et de Dynamique des Systèmes, UMR 5513, 58 Rue Jean Parot, 42023 Saint-Etienne Cedex 2, France ; Assistant professor, Faculty of Engineering, Fukuoka University, Fukuoka, Japan. (Corresponding author), Email: gaochuang.cai@enise.fr;

<sup>3</sup> Lecturer, School of Transportation, Wuhan University of Technology, Wuhan 430063, China.

<sup>4</sup> Associate professor, Laboratory of Solid Structures, University of Luxembourg, Maison du Nombre, 6, Avenue de la Fonte, L-4364 Esch-sur-Alzette, Luxembourg.

<sup>5</sup> Full Professor, Univ Lyon, Ecole Nationale d'Ingénieurs de Saint-Etienne (ENISE), Laboratoire de Tribologie et de Dynamique des Systèmes, UMR 5513, 58 Rue Jean Parot, 42023 Saint-Etienne Cedex 2, France.

<sup>6</sup> Associate professor, School of Civil Engineering, University of Leeds, Woodhouse Lane, Leeds, LS2 9JT, UK.

22 **Keywords:** Seismic behaviour; FRP; Lateral confinement; Plastic hinge region; composite  
23 structure; Hysteresis behaviour

24

## 25 **1. Introduction**

26 It is generally accepted that properly confined concrete can develop adequate ductility for reinforced  
27 concrete (RC) elements allowing sufficient lateral deformability without a significant reduction in  
28 strength. For RC beams and columns, their confinement is usually located at the plastic hinge regions  
29 (PHR) by using different external constraints such as steel tube (Tomii 1985a, 1985b) and fibre  
30 reinforced polymer (FRP) sheet (Teng et al. 2002). Moreover, the confinement can further enhance  
31 the deformability and ductility of RC columns subjected to reversed cyclic loads, which is meaningful  
32 for concrete structures in seismic regions or for high-rise buildings. This is because that unconfined  
33 concrete elements might fail due to damage accumulation during reversed cyclic loads, thus leading  
34 to subsequent further damage or the collapse of whole structure.

35 Fig.1 shows the main confinement methods of two kinds of concrete elements: (i) RC, and (ii)  
36 concrete-filled steel tube (CFST) elements. For the former, the addition of external steel tube  
37 confinement was suggested to improve the ductility, deformation, and damage control of the concrete  
38 cover of RC elements. The concept of “tubed column” was first introduced to the research community  
39 by Tomii et al (1985a,b), which is called as steel tube confined columns. The lateral tubed  
40 confinement at the same time significantly enhances the bearing capacity of the RC elements.  
41 Additionally, the external steel tube can work as a part of the formwork system to quicken the  
42 construction. Since steel tube confined concrete (STCC) elements initially were used in the  
43 construction industry and presents excellent deformation ability and ductility, the research community  
44 has also presented increasing concerns. This can be attributed to the fact that the STCC effectively  
45 avoids the outward local buckling (OLB) for the local yielding of the steel tube under large loads or  
46 at large lateral deformation (Tomii et al. 1985a, 1985b, Sakino et al. 2004), which usually occurs in  
47 CFST elements. This is also because the steel tube is designed not to carry directly axial loads in  
48 STCC elements via the termination of the steel tube at its two ends. Besides, the STCCs provide a

49 solution to overcome the difficulty of the load transfer mechanisms and the detailing design at RC  
50 beam-to-CFST column joint nowadays. Up-to-date, a number of studies have been conducted to  
51 understand the constitutive behaviour (Binici 2005, Li et al. 2005) and structural behaviour of STCCs  
52 under various loads (Aboutaha and Machado 1999). In particular, Han et al. (2005) experimentally  
53 investigated the monotonic and cyclic behaviours of STCC columns, thin-walled STCC column to  
54 beam joints (Han et al. 2009), and thin-walled STCC columns subjected to axial local compression  
55 (Han et al. 2008). Zhou and Liu (2010) experimentally studied the seismic behaviour and shear  
56 strength of STCC short columns, the performance of STCC columns under eccentric compression  
57 (Zhou et al. 2015, Zhou et al. 2016), the behaviour of circle STCC column-to-RC beam connections  
58 under axial compression (Zhou et al. 2017). In addition, Yu et al. (2010) proposed a finite element  
59 method (FEM) analysis model to analyse the mechanisms of STCC columns under axial compression.

60 However, similar to the buckling of the steel tube in CFSTs at large deformation and its corrosion  
61 under aggressive environment limit their application in civil engineering, the corrosion of the steel  
62 tube also obstructs the application of the STCCs in an increasing deteriorative built environment.  
63 According to literature (Wu et al. 2014, Liu et al. 2018), the FRP wrapping of the STCC solves the  
64 durability concerns of the STCC structures. However, a few concerns regarding this kind of structural  
65 elements still need to be addressed such as low longitudinal stiffness and relatively high construction  
66 cost. Therefore, with consideration of these reasons, a FRP-steel confined RC element has been  
67 developed. The first author's research group (Ran 2014, Huang 2016) investigated the constitutive  
68 behaviour of GFRP-STCC under monotonic and cyclic axial loads. Cao et al. (2017) experimentally  
69 investigated the behaviour of FRP-STCC stub columns with expansive self-consolidating concrete  
70 under axial compression. Liu et al. (2018) studied the axial behaviour of circular CFRP-STCC stub  
71 columns. In summary, comparing with STCC and FRP-confined concrete structures, the FRP-STCC  
72 structures are more durable and flexible because of the using of durable FRP materials and a more  
73 effective confinement.

74 On the other hand, CFST elements are popular in high-rise buildings or piers in Europe and Japan as  
75 reinforced concrete is widely applied. This is due to the reasonable arrangement of steel and concrete  
76 in the section, which optimizes the sectional strength and stiffness of the elements leading to an  
77 effective use of the material properties to resist the tension and bending actions in the section.  
78 Meanwhile, the tube can serve as a part of formwork in construction, which decreases labour and  
79 material costs. However, the effects of the bond, confinement, and OLB on CFST's structural  
80 behaviour are under study to facilitate the development of design methods of the members under  
81 lateral reversed cyclic loads. External FRP confining may be a potential solution to fix the OLB  
82 problem of CFST elements (Xiao 2004, Hu et al. 2011) for the high strength and elastic properties of  
83 FRP materials, but which is still under research. Xiao (2004) proposed the FRP-confined CFST  
84 columns, who also compared and commented the FRP-STCC and CFST elements. He concluded that  
85 a FRP-confined CFST column combines the advantages of the conventional CFST column and the  
86 tubed column, in which additional transverse reinforcement is designed for the potential plastic hinge  
87 regions to improve the seismic performance of the elements. In 2005, Xiao et al. (2005) performed a  
88 study to introduce and experimentally validate FRP-confined CFST columns under axial and seismic  
89 loads and confirmed the excellent seismic performance of these columns. Recently, several studies  
90 were reported to examine the constitutive behaviour of FRP-confined CFST columns (Xiao et al.  
91 2005, Liu and Lu 2010, Park et al. 2010, Tao et al. 2011, Lin 2012, Teng et al. 2013, Park and Choi  
92 2013, Hu and Seracino 2013, Wang et al. 2015, Yu et al. 2016), but more studies are underway to  
93 examine details of the elements.

94 Concerning the structural behaviour of FRP-STCC elements under various loads, up to present, there  
95 are only limited studies available in literature. Most of the studies focused on the behaviour of the  
96 elements under axial compressive loads (Cao et al. 2017, Liu et al. 2018). Therefore, the major  
97 objective of this paper is to study the behaviour of circular GFRP-STCC columns under combined  
98 constant axial loads and lateral reversed cyclic loads. Based on experimental observations and  
99 analyses of the deformation mechanisms, this paper also proposes a FEM analysis model to simulate  
100 the structural response under the combined loads. Moreover, this study also aims to discuss the effect

101 of the main structural design factors on the behaviour of FRP-STCC columns under reversed cyclic  
102 loads.

## 103 **2. Experimental program**

### 104 **2.1 Test overview**

105 In this experiment, eight circular sectional concrete columns were designed and prepared, including  
106 one reinforced concrete (RC) column, one steel tube-confined RC column, one steel tube-confined  
107 steel reinforced concrete (SRC) column, one CFRP-steel confined RC column, two GFRP-steel  
108 confined RC columns and two GFRP-steel confined SRC columns. The core concrete diameter of all  
109 specimens was 300 mm and the thickness of the concrete cover was 30 mm. The height of the columns  
110 was 1350 mm with a 300 mm high column head. The dimension details and steel arrangement of the  
111 specimens are presented in Fig. 2. The volumetric ratio of longitudinal steel bar of all specimens was  
112 1.71%, and the stirrup volumetric ratio was 0.6%. For the steel tubes confined specimens, the  
113 thickness of the steel tubes was 3.0 mm. In order to prevent the direct axial compression of the steel  
114 tubes, 20 mm gaps were set at both ends of the columns. In FRP confined specimens, FRP was used  
115 to confine the hinge zone of 500 mm with different layers depending on the test design, while the  
116 remaining parts of the columns were wrapped by 2-layers same-type FRP sheet. For the confined  
117 SRC columns, a standard H-section steel (150mm×150mm×10mm×7mm) was set from underneath  
118 the base beam to the top of the column. Table 1 and Fig.2 (a) show the details of test specimens.

### 119 **2.2 Specimen manufacture**

120 All steel tubes in the study were manufactured from 3.0 mm steel plates by welding at their lap zone.  
121 The tested specimens were prepared following the steps: (1) setting of the reinforcement cage of  
122 columns and base beam; (2) setting of the steel tube (its welding line was placed on the plane oriented  
123 parallel to the column's axis of symmetry); (3) setting of the reinforcement cage and module of the  
124 stigma (column head); (4) curing of the specimens; and (5) removing steel tube for concrete columns  
125 or wrapping FRP sheet for FRP-steel confined concrete columns. The key steps of FRP wrapping  
126 were as follows: (1) polishing their surface with an angle grinder to enhance its surface roughness;

127 (2) clearing the surface of the steel tubes such as wiping them with alcohol; and (3) setting of FRP  
128 sheet. The overlap length of FRP wrapping was about 300 mm and the welding line of the steel tube  
129 was located in the middle of the overlap zone of FRP wrapping to prevent the cracking of welding  
130 line. Fig. 2(b) shows a completely GFRP-steel confined column specimen.

### 131 **2.3 Materials' properties**

132 Two kinds of unidirectional FRP sheets were used, i.e. GFRP sheet L900 ( $900 \text{ g/m}^2$ ) and CFRP sheet  
133 UT70-30 ( $300 \text{ g/m}^2$ ). A construction impregnation adhesive for structural application, an epoxy  
134 adhesive Lica-100 was used, whose properties are listed in Table 2. Ready-mixed concretes were  
135 used, which contained 5-10mm aggregates with a target compressive strength of 40 MPa. According  
136 to the test results of six standard concrete cubes ( $150\text{mm}\times 150\text{mm}\times 150\text{mm}$ ), the cube compressive  
137 strength of concrete was 41.2 MPa, which is approximately transferred as a concrete cylinder'  
138 compressive strength via multiplying by 0.8 for normal strength concrete. The transverse and  
139 longitudinal reinforcements of the columns are 8mm plain (smooth) steel rebars and 16mm deformed  
140 steel rebars, respectively. Q235 steel tube (3.0 mm thickness) was used to confine the columns, whose  
141 properties are listed in Table 2 obtained by the standard test method, GB/T228-2010 (2009). As shown  
142 in Fig. 2, a standard H-section steel ( $150\text{mm}\times 150\text{mm}\times 10\text{mm}\times 7\text{mm}$ ) was used in the tested SRC  
143 columns.

### 144 **2.4 Test setup and measurement**

145 The details of the test setup are illustrated in Fig. 3. The bottom base beam of each specimen was  
146 firstly anchored on a strong RC floor through several high strength steel bolts. At the ends of the  
147 beam, two linear variable differential transducers (LVDTs) were used to record its possible slipping  
148 during the test. The constant axial loads were applied on the top of the columns by a hydraulic jack  
149 with a maximum capacity of 1000 kN, as shown in Fig. 3. The reversed lateral cyclic load was applied  
150 at the column head using a hydraulic jack with a maximum capacity of 1000 kN with a one-way steel  
151 hinge device that can rotate around the vertical and horizontal loading directions. The applied axial  
152 load in each column was designed as 978 kN for RC columns and 1242 kN for SRC columns - about

153 35% of the nominal axial load capacity (N) of the columns obtained as per the Chinese standards (GB  
154 50010-2010 2015, TGJ3-2002 2002).

155 During the tests, the lateral load and displacement of the columns were monitored by using one load  
156 cell and several LVDTs (450 mm, 600 mm, and 750 mm from the top of the base beam), while the  
157 strains of the longitudinal reinforcement, the stirrup, FRP-steel tube and steel tube during the loading  
158 were investigated through several gauges. Four strain gauges (L1~L4) and three hoop strain gauges  
159 (H1~H3) were installed on the longitudinal rebars and on the stirrups at a distance of about 10mm  
160 from the top of the base beam, respectively. Two hoop strain gauges (HN, HS) and three vertical  
161 strain gauges (LN, LS, and LM) were arranged respectively on the surface of the steel tube or the  
162 FRP tube at the distances of 70 mm, 220 mm, and 370 mm from the top of the base beam, in order to  
163 measure the horizontal and vertical strains of the steel tube or the FRP tube.

## 164 **2.5 Loading methods**

165 It is necessary to establish a reasonable loading history to capture the critical issues of the resistance  
166 and deformation on structural elements during the quasi-static cyclic loading tests. After the  
167 application of a constant axial load on top of the columns, a multiple reversed cyclic lateral loading  
168 was performed in each column. In the reference column, a deformation-controlled reversed cyclic  
169 lateral loading was applied with an increment of 4.0 mm. The target deformation of the first cyclic  
170 loading was 4.0 mm. When the lateral displacement arrived at 12mm, the lateral loading was repeated  
171 twice at each target cycle of lateral loading. A similar loading method was performed at the confined  
172 concrete columns, except for that the increment of lateral deformation was set as 8.0 mm after the  
173 lateral displacement of the columns exceeded 16mm. For the security, the tests were finished if the  
174 lateral resistance force of the specimen reduced to 60% of its maximum measured value or the lateral  
175 displacement of the columns is too large such as over 100mm. Fig. 4 presents the loading procedure  
176 applied in the columns.

## 177 **3. Test observations**

### 178 **3.1 Cracking evolution and damages**

179 **(1) RC column and steel tube confined RC column (G0S0T0 and G0S1T0)**

180 In Specimen G0S0T0, the first horizontal crack occurred at the north side of the column about 100  
181 mm from the top of the base beam. Then, a semi-circular horizontal crack appeared on the south side  
182 with a height of 100 mm. At the same time, a second crack appeared at a north side of the column, at  
183 a height of 200 mm. Meanwhile, horizontal cracks began to appear in the upper part and in the middle  
184 of the south side and began to develop to the north side of the column. Next, new horizontal cracks  
185 appeared in the columns about 400 mm and 600 mm from the top of the base beam. With the increase  
186 of the lateral displacements, the cracks below the south side developed, while the horizontal cracks  
187 continued to develop, and crushing of the concrete at the south side of columns occurred. At this time,  
188 the first vertical crack was confirmed in the south side concrete along with the crushing of the concrete  
189 on the north side. Next, at the north side of the concrete first vertical cracks appeared. When the lateral  
190 displacement was about 24 mm, the concrete cover on the north side shows a large area of spalling  
191 but a buckling of the longitudinal reinforcing bar could not be observed. All the damages and cracks  
192 in the column were mainly caused by the plastic deformation of concrete and internal damage  
193 surrounding the deformed reinforcements. The final failure morphology of the specimen is shown in  
194 Fig. 5.

195 In the steel tube confined RC column, G0S1T0, the early stage cracks cannot be visually observed  
196 due to the external steel tube. When the lateral displacement was 48mm, the cracking and the  
197 extrusion exfoliation of concrete were found at the bottom of the column. After removing the steel  
198 tube at the end of the column, the concrete at the bottom of the confined zone was crushed, but due  
199 to the constraints of the steel tube, it did not fall off. Several slipped shear cracks were also found at  
200 the foot of the column. All of damages and cracks were still caused by the plastic deformation of the  
201 elements, however, the confinement of steel tube effectively reduces the crushing of the concrete  
202 which indicates the failure of the column will be difference with that of RC columns in which the  
203 sectional concrete crushing is one of main reasons of structural failure.

204 **(2) FRP-steel confined RC columns (G5S1T0, G7S1T0 and C7S1T0)**

205 Specimen G5S1T0 presented a large residual displacement after testing. At the surface of GFRP tube  
206 wrapped in the column foot, the resin slightly cracked. After removing of the GFRP wrapping and  
207 steel tube, several cracks were found at the column foot and the south side of the column. This can  
208 be explained by the fact that the compression from the upper part of the north side GFRP-steel  
209 confined concrete promotes the crushing to the below concrete (about 50 mm from the top of the base  
210 beam). However, the damage of the outermost layer of GFRP tube did not appear during testing.  
211 Compared to Specimen G5S1T0, two more layers of GFRP sheets were applied in Specimen G7S1T0,  
212 but the failure mode of the two specimens is similar. When the lateral displacement was too large, the  
213 concrete at the top of the base beam was disintegrated. By removing the GFRP tube and steel tube  
214 after testing, several horizontal and diagonal cracks were observed at the distance of 100 mm from  
215 the top of the base beam. However, the confinement of the GFRP was able to protect the core concrete  
216 in a satisfactory manner. Comparing with Specimen G7S1T0, when GFRP was replaced by CFRP,  
217 similar failure mode, cracking pattern, and damages were found in Specimen C7S1T0, so that it can  
218 be stated that the confinement of the columns were performant. In summary, the main damages and  
219 cracks of FRP-steel confined RC columns concentrated on the critical section between the column  
220 and the base beam, which were expressed as crushing and slipped cracks, respectively.

### 221 **(3) FRP-steel confined SRC columns (G0S1T1, G5S1T1 and G7S1T1)**

222 The cracks and damages of the steel tube confined SRC column G0S1T1 were similar to that of the  
223 steel tube confined RC column G0S1T0. When the lateral displacement increased to about 48mm, the  
224 parts of the concrete on the top of the base beam and the column foot were cracked and damaged as  
225 the steel tube deformation and stretched continuously. At the end of the test, there was no apparent  
226 buckling or other failure characteristics visible on the steel tube. When removing the steel tube later,  
227 a horizontal crack was observed at about 80 mm near the column foot but no other damages to the  
228 column body. When the steel tube was confined by GFRP tube such as Specimen G5S1T1, the cracks  
229 appeared on the south side of the column above the base beam when the lateral displacement of the  
230 column was 25mm. These cracks developed further into compressive damage of the concrete cover.

231 At the end of the experiment, however, the confined concrete is still almost intact. Comparing with  
232 the case of Specimen G5S1T1, the cracks and damages were controlled well when using more layers  
233 of GFRP sheets in G7S1T1. However, the failure mode of this specimen was similar to that of  
234 Specimen G5S1T1. In the case of large displacement, the concrete at the top of the base beam was  
235 initially disintegrated, before being damaged near the top of the column. At last, the concrete was  
236 damaged at around 10 mm over the base beam, while the confined concrete remained protected  
237 without visual horizontal or diagonal cracks. In summary, the damages and cracks in the confined  
238 SRC columns were much smaller than those of the other columns, which is attributed to the  
239 reinforcement of the strong H-sectional steel inside.

## 240 **3.2 Hysteresis behaviour**

### 241 **(1) RC and steel tube confined RC columns (G0S0T0 and G0S1T0)**

242 Regarding the RC column, the lateral load-displacement curve is almost linear at the initial stage of  
243 loading. At the second cycle of the same target deformation, the stiffness and lateral load-bearing  
244 capacity of the specimen hardly degraded. However, the residual deformation became larger and the  
245 unloading stiffness and bearing capacity decreased with the increase of the lateral displacement, but  
246 the pinch contraction phenomenon of the hysteresis hoops was not obvious. When the displacement  
247 was 24 mm, the test was stopped due to the large area of concrete spalling. At this moment, the lateral  
248 load was 73.4% of the axial peak load of the column. For specimen G0S1T0, the residual deformation  
249 during unloading was small at the beginning. The stiffness and the bearing capacity of the specimen  
250 at the early stage are not significantly decreased at the same deformation level. As shown in Fig. 6,  
251 the hysteretic pinch phenomenon was also not obvious in this column showing that it has a strong  
252 energy dissipation capacity. When the lateral displacement was 72mm, the lateral load decreased to  
253 62% of its peak load.

### 254 **(2) FRP-steel confined RC columns (G5S1T0, G7S1T0 and C7S1T0)**

255 Regarding specimen G5S1T0, the lateral load and stiffness of the specimen have not changed and its  
256 residual deformation was small at the initial stage. However, as shown in Fig. 6, with the increase of

257 lateral displacement, the hysteresis loop appears an obvious pinch and shrink phenomenon, but the  
258 shape of the loop is still fat. The bearing capacity of the column did not decrease rapidly after reaching  
259 the peak load indicating that the ductility of the column was satisfactory. For specimen G7S1T0, the  
260 shape and variation of the hysteresis curve were very similar to that of G5S1T0, however, the  
261 hysteresis loop of the G7S1T0 was fatter. For specimen C7S1T0, its residual deformation was small  
262 while the stiffness and bearing capacity had almost no degradation when the displacement was small.  
263 As the displacement increased, the residual deformation of the specimen increased, and the stiffness  
264 and bearing capacity decreased obviously.

### 265 (3) FRP-steel confined SRC columns (G0S1T1, G5S1T1 and G7S1T1)

266 As it can be seen from Fig. 6, G0S1T1 specimen shows a fusiform hysteresis loop at the initial stage,  
267 while the hysteresis curve is gradually getting fatter with the increase of the displacement and shows  
268 no sign for the pinch-and-shrink phenomenon. This demonstrates that the column possesses an  
269 excellent energy dissipation ability. For specimen G5S1T1, its bearing capacity and stiffness did not  
270 significantly change under the same displacement. With the increase of loading, the shape of the  
271 hysteresis loop tended to become fatter. The degradation rate of the lateral load was small after the  
272 column reached its peak load meaning that the column has a satisfactory ductility. For specimen  
273 G7S1T1, the residual deformation of the column during the initial loading was quite small. Similar  
274 to that of G5S1T1, no obvious degradation occurred in the stiffness and lateral load of the specimen  
275 at the same level of lateral displacement. With the increase of lateral displacement largely, the  
276 hysteresis curve of the specimen become fatter showing its strong energy dissipation capacity.  
277 Comparing between G7S1T1 and G5S1T1, no significant difference was observed in G7S1T1  
278 indicating that increasing the number of GFRP layers has no influence on the seismic performance of  
279 the SRC columns.

### 280 3.3 Strain evolution of reinforcing rebars and steel tube

281 Fig. 7 demonstrates that when the lateral load increases, the strain of the steel rebars increases as the  
282 lateral displacement of RC column and steel tube confined RC columns. When the displacement was

283 32 mm, the longitudinal reinforcement in L2 has a strain of higher than its yielding strain, i.e.  $2000\mu\epsilon$ .  
284 With the increase of the lateral displacement, the longitudinal reinforcement begins to yield. However,  
285 the maximum compression strain of the longitudinal reinforcement reached  $2500\mu\epsilon$  at the later  
286 loading stage indicating that it did not undergo significant plastic deformation. The figure shows that  
287 the stirrups can confine the concrete well in the circular RC column.

288 As shown in Fig. 7, taking specimen G7S1T0 as an example with the FRP-steel confined RC columns,  
289 the maximum strains of the steel tube occurred at the top of the base beam in both sides are  $6602\mu\epsilon$   
290 and  $3543\mu\epsilon$  - both exceeding the yielding strain of the tube. The hoop strain on the outside tube  
291 confirmed that the steel tube were in tensile. Similar to the variation law of longitudinal strain, the  
292 amplitudes of HN50 and HS50 close to the top of the base beam were  $4883\mu\epsilon$  and  $4883\mu\epsilon$ ,  
293 respectively. Specimen G0S1T1 shown a similar strain evolution to Specimen G7S1T0. For FRP-  
294 steel confined SRC column G5S1T1, the strains of LN50 and LS50 near the base beam were  $6823\mu\epsilon$   
295 and  $5949\mu\epsilon$ , respectively. All the results of strain gauges indicated the steel hoop were under tension.  
296 This is due to the expansion of the core concrete after multiple lateral reserved loads leading to an  
297 increase in the deformation of steel tube confined by GFRP sheet. At the same time, HN50 and HS50  
298 located on the south and north sides were  $6755\mu\epsilon$  and  $4799\mu\epsilon$ , respectively which reached its yielding  
299 status. In summary, in the FRP-steel confined SRC columns, at the same section of the column foot,  
300 the strain on the north side, the south side, and the neutral axis were all different, which means that  
301 the hoop strain distribution was not uniform. The strain of the steel tube in the confined SRC columns  
302 was smaller than that of other specimens because the sectional rigidity of the SRC column is quite  
303 large for the using of H-section steel.

## 304 **4. Comparison and analyses**

### 305 **4.1 Comparison of hysteresis behaviour**

306 Fig. 8 compares the hysteresis curves of all the tested specimens. Results show that the bearing  
307 capacity and ductility behaviour of specimen G0S1T0 was better than that of the specimen G0S0T0

308 owing to the external lateral confinement of steel tube. Comparing to Specimen G0S1T0, an overall  
309 improved bearing capacity, ductility, and energy dissipation capacity of the steel tube confined RC  
310 column was obtained by the GFRP wrapping, such as the specimens G5S1T0 and G7S1T0.  
311 Furthermore, with the increase of the number of layers of FRP sheet, the enhancement effect of GFRP  
312 wrapping was more obvious.

313 Examining the case of the specimens G5S1T0 and G7S1T0, the seismic performance of the FRP-steel  
314 confined RC columns was improved with the number of layers of FRP sheet, but the enhancement  
315 effectiveness became lower with the number of FRP layers. For the specimens G7S1T0 and C7S1T0,  
316 although the lateral confinement (both the lateral confinement stiffness and strength) of the CFRP  
317 was stronger than that of the GFRP, the load-carrying of the specimen G7S1T0 is slightly better than  
318 the specimen C7S1T0. This can be explained as follows: (a) the failure mode of the confined RC  
319 columns was controlled by the damages and cracks in the confined RC, but not controlled by the  
320 rupture of the FRP wrapping usually occurred in axial compressive columns, which indicated that the  
321 FRP material were not fully utilized; (b) this little abnormal case may be induced by the manufacture  
322 error of the specimens, and testing error etc.

323 For GFRP-steel confined RC/SRC columns, it was observed that the bearing and deformation  
324 capacities of the specimen G5S1T1 (or G5S1T0) were improved when using GFRP to confine steel  
325 tube, comparing with the ones of specimen G0S1T1 (or G0S1T0). This indicates that the FRP-steel  
326 composite tube can improve the seismic performance of the RC/SRC columns in an effective manner.  
327 However, when the used amount of steel reinforcement (H-section steel, steel reinforcing bars, and  
328 steel tube) was high, the improvement caused by FRP wrapping became not obvious. For the  
329 specimens G5S1T1 and G7S1T1, the increase of the number of layers of FRP did not improve  
330 significantly the shear-resistance and the deformation capacity of the confined SRC columns. This  
331 could be explained by the fact that the confined columns using H-section steel already have a high  
332 seismic performance indicating that the confinement effectiveness from FRP sheets was not  
333 developed.

## 334 4.2 Skeleton curves-deformation and ductility

335 Skeleton curves can clearly reflect the bearing capacity and ductility of RC members which are the  
336 main considerations of the seismic design of the members. Generally, a skeleton curve mainly  
337 includes three characteristic points: yield strength point, peak strength point, and ultimate strength  
338 point. The peak point is the peak load of the columns,  $P_{max}$ . For the FRP-steel confined RC columns,  
339 the ultimate point is the point at 85% of the peak load ( $85\% P_{max}$ ),  $P_u$ . The deformability of FRP-steel  
340 confined SRC columns was excellent; however, the ultimate deformation was large when the lateral  
341 load drop is not obvious. Due to safety reasons, all tests were stopped before reaching the ultimate  
342 state of the columns. For a comparative analysis, the ultimate strength points of two FRP-steel  
343 confined SRC columns (Specimens G5S1T1 and G7S1T1) were considered as a point when the lateral  
344 load drops to 90% of its peak load in this study.

345 There is no uniform the calculation method to adjust the yield point of the concrete element. In this  
346 paper, the equivalent elastoplastic energy absorption method (Park 1988) was applied to define the  
347 yielding point by introducing an additional line in the load-deformation curve such as to define an  
348 equivalent elastoplastic displacement with the same energy dissipating, as shown in Fig. 9: the  
349 trapezoidal OABC area is equal to the area encircled by the curve ODBCO. In this figure,  $\Delta_u$  and  $P_u$   
350 represent the ultimate displacement and the ultimate load, respectively;  $P_y$  and  $\Delta_y$  are the yield load  
351 and displacement, respectively.  $P_{max}$  is the peak load and  $\Delta_{max}$  is the corresponding displacement.  $P_u$   
352 is taken as  $85\%P_{max}$  or  $90\%P_{max}$  depending on columns with/without H-section steel with the  
353 exception of Specimen G0S1T1 ( $85\%P_{max}$ ).  $R$  is the drift angle of the columns.

354 Fig. 10 shows the comparison of the skeleton curves of all the tested specimens and Table 3 presents  
355 a summary of all test results. The yield loads of FRP-steel confined RC columns without H-section  
356 steel increased slightly with the number of layers of FRP wrapping. The yield displacement for the  
357 steel tube confined or FRP-steel confined RC columns was larger than that of RC columns. Compared  
358 to Specimen G0S1T0, G5S1T0 and G7S1T0 have a larger yield load which increased by 5.6% and  
359 11.0%, respectively. The peak loads of the specimens G5S1T0 and G7S1T0 increased by 10.2% and  
360 16.0%, respectively, while their peak displacements increased by 14.9% and 28.4%, respectively, and

361 their ductility coefficients increased by only 0.5% and 3.1%, respectively. This indicates that the  
362 ultimate shear capacity and deformation capacity of the steel tube confined RC column were  
363 significantly improved after confinement by FRP wrapping, while no significant improvement was  
364 achieved for its ductility. On the other hand, CFRP-steel confined specimen (C7S1T0) had a better  
365 ductile coefficient which was higher than that of GFRP-steel confined specimen (G7S1T0) because  
366 the confinement of the CFRP was stronger than that of the GFRP, as the same number of layers of  
367 FRP was used.

368 With regard to the specimens using H-section steel, similar results were obtained. Comparing to the  
369 specimens G0S1T1, with an increase of the number of GFRP layers, the yielding load of the  
370 specimens G5S1T1 and G7S1T1 increased slightly by 0.3% and 10.2%, their peak load increased by  
371 8.8% and 17.9% and their ultimate displacement increased by 7.1% and 12.9%, respectively.  
372 Meanwhile, the ductility coefficients of the G5S1T1 and the G7S1T1 also increased slightly with  
373 increasing the number of GFRP layers.

374

### 375 **4.3 Stiffness degradation**

376 The lateral stiffness of RC columns generally degrades under a reversed cyclic loading for several  
377 reasons such as the decreasing of effective compression area of columns caused by concrete cracking  
378 and the yielding of steel reinforcement etc. The stiffness in this study refers to an equivalent lateral  
379 stiffness, which is the average value of the load-displacement ratios at the unloading points in the  
380 positive and negative directions of the first loading hoop of each target displacement level. Fig. 11  
381 demonstrates the stiffness degradation curve of all specimens. Results show that the initial stiffness  
382 of the RC column (G0S0T0) is low, while the members confined by steel tube or FRP-steel tube have  
383 a much higher stiffness. As the lateral displacement increases, the stiffness of the confined RC  
384 columns degraded slowly. In addition, the stiffness degraded more slowly when the number of GFRP  
385 layers increased. The initial stiffness of specimens G0S1T1, G5S1T1, and G7S1T1 are almost the  
386 same due to all SRC columns have a strong stiffness. As the lateral displacement increased

387 continuously, the degradation rates of the lateral stiffness of the SRC specimens remained an almost  
388 identical value.

#### 389 **4.4 Energy dissipation capacity**

390 The energy dissipation capacity of RC elements is an important index to evaluate their capacity to  
391 absorb earthquake energy induced by ground shaking. The failure and collapse of RC structures could  
392 happen due to poor energy dissipation during an earthquake. In this study, the cumulative energy  
393 dissipation was calculated considering only the first load hoop at the corresponding displacement  
394 level. As shown in Fig. 12, the accumulated energy dissipation of RC columns is less than that of the  
395 confined RC columns at the same lateral displacement. As the number of GFRP layers increased, the  
396 energy dissipation capacity of the confined columns increased. However, the accumulated energy  
397 dissipation of the G7S1T0 was only slightly higher than that of the G5S1T0. This is because the  
398 specimen G5S1T0 wrapped with 5 layers of GFRP may be already under an over-confining state.  
399 Therefore, the effect of increasing GFRP layers on energy dissipation may be small in G7S1T0.  
400 Similarly, the specimen C7S1T0 got a greatly improved energy dissipation capacity comparing to the  
401 specimen G0S0T0, but when comparing to the specimens G7S1T0 and G5S1T0, their energy  
402 consumption capacity was almost the same.

403 For the SRC columns (G0S1T1, G5S1T1, and G7S1T1), similar behaviour was obtained: (1) in the  
404 initial stage, the accumulated energy dissipation of the specimens was similar for all the specimens;  
405 (2) as the lateral displacement increased, the energy dissipation capacity of the columns increased and  
406 shown a different evolution and finally the energy consumption of the G7S1T1 is highest; and (3) the  
407 number of GFRP layers has no significant influence on the energy dissipation capacity of the SRC  
408 columns. This again shows that the improvement of the seismic performance of the SRC columns due  
409 to an increasing the number of layers of GFRP sheet is relatively small.

#### 410 **5. FEM simulation of FRP-steel confined RC columns**

411 According to Section 4, the GFRP wrapping did not present its positive effect on the seismic  
412 performance of the SRC columns. The main reason could be that the core SRC column possessed

413 already a high stiffness to the lateral deformation under the reversed cyclic loads. Therefore, in this  
 414 section, the paper emphasizes on the simulation of FRP-steel confined RC columns. OpenSees  
 415 (Mazzoni et al. 2006), as an open source object-oriented software, is used for the analysis of the tested  
 416 RC and FRP-steel confined RC columns. The basic assumptions for the analyses of the columns  
 417 include: (a) concrete section remained a plane and normal to the neutral axis after bending, (b) the  
 418 slippage between steel rebar and concrete was neglected to simplify the simulation, and (c) the shear  
 419 effect was neglected to simplify the simulation due to the fact that the shear span ratios of all columns  
 420 in this FEM is not less than 2 (especially most case is 4), which indicated the flexural failure mode  
 421 will occur in the columns and the shear effect would be relatively small. In the following sections,  
 422 the geometric and materials models used in the program are discussed.

## 423 5.1 Material model and cross-section rule

### 424 5.1.1 Concrete and steel tube confined concrete

425 For the RC column, a three-line constitutive model proposed first by Kent and Park (1971) and  
 426 modified by Scoot et al. (1982) was selected as a backbone curve for concrete material. The backbone  
 427 and hysteresis model of concrete (uniaxial materials of Concrete01 in OpenSees) are presented in Fig.  
 428 13 (Mazzoni et al. 2006). The related equations of the model are as follows:

$$429 \quad f = \begin{cases} Kf_{co} \left[ 2 \left( \frac{\varepsilon}{\varepsilon_{cc}} \right) - \left( \frac{\varepsilon}{\varepsilon_{cc}} \right)^2 \right], \varepsilon \leq \varepsilon_{cc} \\ Kf_{co} \left[ 1 - Z \left( \frac{\varepsilon}{\varepsilon_{cc}} \right) \right], \varepsilon_{cc} \leq \varepsilon \leq \varepsilon_{cu} \\ 0.2Kf_{co}, \varepsilon \geq \varepsilon_{cu} \end{cases} \quad (1)$$

430 In the equation,

$$431 \quad K = 1 + \rho_v f_{yh} / f_{co} \quad (2)$$

$$Z = \frac{0.5}{\frac{3 + 0.29 f_{co}}{145 f_{co} - 1000} + 0.75 \rho_v \sqrt{\frac{b}{s}} - 0.002K} \quad (3)$$

432 Where,  $\varepsilon_{cc}$  is the strain corresponding to the peak stress of the confined concrete, taken as 0.002K; K  
 433 is the coefficient of the increase of the peak load caused by the confinement. Z is the slope of the  
 434 strain drop curve;  $f_{co}$  is the compressive strength of standard non-confined concrete cylinders;  $f_{yh}$  is  
 435 the yield strength of stirrups;  $\rho_v$  is the volumetric reinforcement ratio of stirrups; b is the width of core  
 436 concrete; s is the spacing of stirrup. For steel tube confined RC columns, the analysis of the confined  
 437 concrete of the columns adopted the constitutive model of steel tube confined concrete proposed by  
 438 Lin (2012).  
 439

#### 440 **5.1.2 FRP-steel confined concrete model**

##### 441 **a. Monotonic model**

442 An analysis-oriented stress-strain model for FRP-steel confined concrete was used in this paper.  
 443 Referring to analysis-oriented models for FRP-confined concrete (Jiang et al. 2007), a passive  
 444 confining stress-strain model for FRP confined concrete in FRP-steel confined concrete columns can  
 445 be achieved from an active confining model for concrete through an incremental approach. The model  
 446 is proposed on the assumption that the axial stress and strain of FRP confined concrete at a given  
 447 hoop strain are the same as those of the same concrete confined actively with a constant confining  
 448 pressure equalling to that provided by the FRP wrapping (Jiang et al. 2007). The following axial  
 449 stress-strain model for concrete, which was built by Popovics (1973), is adopted in this paper.  
 450 Popovics (1973) proposed a stress-strain model for the confined concrete with an active confining,  
 451 which presents a great analysis accuracy. Thus, this study suggests to use it to analyse the stress-strain  
 452 of GFRP-steel confined concrete elements, which is given as:

$$453 \quad \frac{\sigma_c}{f_{co}} = \frac{(\varepsilon_c / \varepsilon_{cc}) \cdot r}{r - 1 + (\varepsilon_c / \varepsilon_{cc})^r} \quad (4)$$

$$454 \quad r = \frac{E_c}{E_c - f_{cc} / \varepsilon_{cc}} \quad (5)$$

455 Based on the research conducted by the research group of the first author of the paper (Lin 2012, Ran  
 456 2014, Huang 2016), the study suggests to consider the active (stirrups and steel tube) and passive  
 457 confining actions (FRP wrapping) in FRP-steel confined concrete columns to model the peak axial  
 458 stress and the corresponding axial strain of FRP-steel confined concrete. The proposed models are  
 459 expressed as:

$$460 \quad \frac{f_{cc}}{f_{co}} = 1 + 4.08 \left( \frac{f_{lf}}{f_{co}} \right)^{1.28} + 5.5 \left( \frac{f_{ls} + f_{lh}}{f_{co}} \right)^{0.86} \quad (6)$$

$$461 \quad \frac{\varepsilon_{cc}}{\varepsilon_{co}} = 2 + 11.72 \left( \frac{f_{lf}}{f_{co}} \right)^{0.55} + 5.8 \left( \frac{f_{ls} + f_{lh}}{f_{co}} \right) \quad (7)$$

462 Referring to the confining mechanism of FRP confined CFST elements proposed by Hu (2011), in  
 463 this study, the relationship between hoop strain ( $\varepsilon_h$ ) and axial strain of confined concrete is calculated  
 464 as:

$$465 \quad \frac{\varepsilon_{cc}}{\varepsilon_{co}} + 0.66 \left( 1 + 8 \frac{f_1}{f_{co}} \right) \times \left\{ \left[ 1 + 0.75 \left( \frac{\varepsilon_h}{\varepsilon_{co}} \right) \right]^{0.7} - \exp \left[ -7 \left( \frac{\varepsilon_h}{\varepsilon_{co}} \right) \right] \right\} = 0 \quad (8)$$

466 In the equations,  $f_{cc}$  is the compressive stress of confined concrete;  $f_{ls}$ ,  $f_{lf}$  and  $f_{lh}$  are the confining  
 467 stresses of steel tube, FRP and stirrups, respectively;  $f_1$  is the total confining pressure;  $E_c$  is the elastic  
 468 modulus of concrete, which is taken as  $4736f_{co}^{0.5}$ ;  $\varepsilon_{cc}$  is the axial strain of confined concrete at its  
 469 strength;  $\sigma_c$  is the axial stress of tested concrete specimen;  $\varepsilon_{co}$  is the axial strain of concrete at its  
 470 strength;  $\varepsilon_c$  is the unit strain of concrete corresponding to  $\sigma_c$ .

471 As an analysis-oriented stress-strain model, the generation of the axial stress-strain curves for FRP-  
 472 steel confined concrete would be achieved by an incremental process, which was introduced detailed  
 473 in literature studied by the research group of the first author of the paper (Huang 2016).

#### 474 **b. Multi-cycle model**

475 The cyclic constitutive model includes mainly the skeleton model and hysteretic law. The latter has  
 476 two key unloading and reloading paths, and the calculation of plastic strain and stress degradation.

477 Here, the monotonic model proposed above is used to simulate the skeleton curve of the FRP-steel  
478 confined RC columns under cyclic loading. For the hysteretic models, considering the fact that the  
479 strength ratio of the FRP materials to steel is fairly large, the confining effectiveness of FRP-steel  
480 tube to the concrete is considered similar to that of the FRP-confined concrete. Meanwhile, due to the  
481 existence of the steel tube and transverse rebars in the FRP-steel confined RC columns, the authors  
482 suggest to use an improved model proposed by Lam and Teng (2009). The key features and related  
483 equations are presented in Fig. 14. The details of the multi-cyclic model are reached in the reference  
484 (Huang 2016).

### 485 **5.1.3 *A new material constitutive model for FRP-steel confined concrete developed with*** 486 ***an OpenSees Programming***

487 An accurate material constitutive model is the base of the analysis of the RC columns subjected to  
488 reversed cyclic loads. OpenSees is a well-known open source platform with a strong nonlinear  
489 structural analysis and a high compatibility. FRP-steel confined concrete can significantly improve  
490 the seismic behavior of the RC columns as demonstrated in Section 4 of the paper. However, the  
491 existing material constitutive models for FRP-steel confined concrete are not available in the current  
492 version of OpenSees. By the C++ programming language, a new user-defined material constitutive  
493 model based on the monotonic and multi-cycle constitutive model proposed in Section 5.1.2 was  
494 developed, and applied into an OpenSees platform. The developed new material constitutive model  
495 is suitable for FRP-steel confined concrete in circular section. The material models and elements are  
496 separate and independent in OpenSees. Therefore, all existing elements in OpenSees can be  
497 compatible with the new material model. Compared with the existing concrete model, the new  
498 developed material model can accurately simulate the true stress-strain relationship of FRP-steel  
499 confined concrete, especially the unloading rules including residual strain, which would improve the  
500 pinching effect of FRP-steel confined RC columns.

501

### 502 **5.1.4 *Steel model***

503 In this study, a constitutive model of steel reinforcement proposed by Menegotto and Pinto (1973)  
504 was used considering steel reinforcement as an elastic-perfectly-plastic material, which is given as:

$$505 \quad \sigma^* = b\varepsilon^* + \frac{(1-b)\varepsilon^*}{(1+\varepsilon^{*R})^{1/R}} \quad (9)$$

506 where,  $b$  is strain hardening coefficient;  $\sigma^*$  and  $\varepsilon^*$  are normalized stress and strain.  $R$  is a curvature  
507 parameter. The detailed calculations of the parameters are available in the references (Menegotto and  
508 Pinto 1973, Orakcal et al.2006). Fig. 15 depicts a typical hysteretic stress–strain response output for  
509 steel reinforcement.

### 510 **5.1.5 Cross-section rule**

511 A distributed-plasticity, force-based nonlinear beam-column element was selected for the analysis of  
512 all columns. For FRP-steel confined RC columns, two beam-column elements were used to simulate  
513 the FRP confined hinge zone of 500 mm height and the remaining part of the column, respectively,  
514 which was described in Section 2.1. Similarly, two beam-column elements with the same element  
515 size were used for RC columns or steel tube confined RC columns. A cantilever half-column model  
516 was used in this simulation, which was used to be tested in this paper. As described in Section 2.1,  
517 the steel tubes and the FRP wrapping were terminated at their two ends to avoid the direct axial  
518 compression. Therefore, the steel tube and the FRP wrapping in the confined RC columns mainly  
519 provide the confining effect for the concrete core. In order to simply the simulation, the models of the  
520 stirrup, the steel tube and the FRP wrapping in the confined RC columns were not built in this paper,  
521 while the confining effects of the three parts on the concrete core were considered by introducing the  
522 above proposed stress-strain relationship of FRP-steel confined RC into the element, as demonstrated  
523 by Fig. 16. The circular cross-section of all columns was divided into 36 parts in hoop direction and  
524 30 parts in radial direction. Therefore, 1080 fibers were used in the paper. The 1080 fibers (36\*30  
525 fibers) were determined according to the balance between computational accuracy and computational  
526 efficiency before ensuring convergence. However, a convergence study regarding the element size  
527 and fiber number was not conducted in this paper.

## 528 **5.2 FEM model validation**

529 Fig. 17 presents a comparison between the simulated and tested results of RC column and FRP-steel  
530 confined RC columns. It can be seen that the peak load of the simulated curves are very similar to  
531 their measured values, and the corresponding lateral displacements were also consistent with the test  
532 results. For the FRP-steel confined RC columns, the simulated curves were in good agreement with  
533 their experimental curves. Although a new material constitutive model for FRP-steel confined  
534 concrete, which would improve the pinching effect of the columns, was implemented in the analysis,  
535 the pinching effect of the simulated curves is still more obvious than that of the test curves, especially  
536 for the specimens G5S1T0, G7S1T0 and C7S1T0. This may be due to the fact that the slippage of  
537 steel rebar and concrete is not considered, which was neglected to simplify the simulation in this  
538 paper. Overall, the simulation results were in good agreement with the experimental results. Therefore,  
539 it is feasible to use the OpenSees-based FEM model to simulate the seismic performance of FRP-steel  
540 confined RC columns.

## 541 **5.3 Parametric study of FRP-steel confined RC columns**

542 To proper the seismic design of FRP-steel confined RC columns, it is necessary to understand the  
543 influence of main parameters on the seismic performance of the columns to make reliable adjustments  
544 accordingly based on laboratorial study. In this study, a parametric study was carried out on the effects  
545 of various parameters on the seismic preformation of FRP-Steel confined RC columns. The basic  
546 models from the above simulation program were used. The main structural parameters studied were  
547 axial load ratio (0.1-0.8), shear span ratio (2-10), steel tube thickness (1-6 mm), longitudinal steel  
548 ratio (change steel diameter), the number of FRP layers (1-8 layers), and the wrapping height of FRP  
549 sheet in the columns (0-1000 mm).

### 550 **5.3.1 Effect of axial load ratio**

551 Based on the tested specimens G0S1T0 and G5S1T0, the axial load ratio ranges from 0.1 to 0.8, as  
552 shown in Fig. 18, and the results demonstrate that during the increase of axial load, the bearing  
553 capacity of the specimens under reversed cyclic loads also increases. However, the bearing capacity

554 of the specimens decreased with an increased axial load more rapidly in post-peak. This shows that  
555 the ductility got lower as the axial load ratio increased. The specimen G5S1T0 confined by 5-layer  
556 GFRP sheet showed a better ductility than that of the specimen G0S1T0 confined only by steel tube.

### 557 **5.3.2 Effect of shear span ratio**

558 Fig. 19 demonstrates the impact of shear span ratio on the seismic behaviour of the specimens  
559 G0S1T0 and G5S1T0 without changing the other conditions. Results show that the effect of the shear  
560 span ratio is basically the same when different types of external lateral confinement are used. As the  
561 shear span ratios increased, the bearing capacity of the specimens decreased in turn. The peak  
562 displacement also increased when shear span ratio increased meaning that the flexural capacity of the  
563 columns was stronger.

### 564 **5.3.3 Effect of the thickness of steel tube**

565 Fig. 20 shows the results when the thickness of steel tube increased from 1 mm to 6 mm in the  
566 specimens G0S1T0 and G5S1T0, respectively. It is observed that as the thickness of steel tube  
567 increased, the ductility and load carrying capacities of the specimens were improved. Moreover,  
568 changing the thickness of steel tube has a greater influence on the specimen G0S1T0, as its bearing  
569 capacity and ductility have been improved more significantly, and its peak strain became higher. On  
570 the other hand, due to the lateral confinement of five layers of GFRP sheet was considered over-  
571 confining, the effect of the thickness of steel tube on the specimen G5S1T0 was not very significant.  
572 It is observed that when using FRP-steel tube to confine RC columns in practice, it is not advisable  
573 to increase the thickness of steel tube in order to get a stronger confinement. It should be considered  
574 that the simply increasing of the tube thickness would increase the self-weight of the structures, which  
575 is not ideal for resisting the seismic actions.

### 576 **5.3.4 Effect of longitudinal steel ratio**

577 The effect of longitudinal steel ratio on the seismic behaviour of FRP-steel confined RC columns was  
578 examined by increasing the diameter of longitudinal reinforcement ( $D$ ) of reference specimens. As

579 shown in Fig. 21, the results show that the bearing capacity of the two specimens is improved when  
580 the reinforcement ratio of longitudinal reinforcement increases, but the influence on the degradation  
581 ratio of the lateral load of the columns in post-peak is not obvious.

### 582 **5.3.5 Effect of the layer number and confining height of FRP sheet**

583 The effect of the number of FRP layers on the load-displacement skeleton curve of the columns is  
584 shown in Fig. 22. It was obtained that the lateral ultimate load and its corresponding displacement of  
585 the column increased as the number of GFRP layers increased. This indicates that as the number of  
586 GFRP layers increases, the bearing capacity and ductility of the columns is increased. On the other  
587 hand, based on the results of the specimen G5S1T0, the increase of the confining height of GFRP  
588 sheet (0, 300, 500, 800, and 1000 mm, respectively) has no significant effect on the bearing capacity  
589 and ductility of the specimens after the height reaches 300 mm. The height exceeds over 1.5 times of  
590 the diameter of the columns which is similar to the case in RC elements reported before. Therefore,  
591 the confining height of circular FRP-steel confined RC columns is suggested as 1.5 times of the  
592 column's diameter, which can make the columns achieve an economical and reasonable lateral  
593 confinement.

## 594 **6. Discussions**

### 595 **6.1 Plastic Hinge Region (PHR) height**

596 The predication of the lateral load–deformation behaviour of a concrete column involves an important  
597 step, modelling the plastic hinge region (PHR) of the column (e.g. Inel and Ozmen 2006, Youssf et  
598 al. 2015, Yuan et al. 2017). The region is defined as the deformation and damage region of elements,  
599 which experience inelastic demands. Based on the literature, previous experimental studies on  
600 concrete columns (unconfined or confined) assessed the PHR height by observing visually the  
601 damage regions at both ends of the columns (e.g. Bae and Bayrak 2008, Liu and Sheikh 2013). The  
602 damages mainly include cracks and spalling of concrete cover, which usually was considered that it  
603 relates to the longitudinal plastic deformations of the columns. For FRP confined concrete elements,

604 Ozbakkaloglu and Sattcioglu (2006, 2007) recommended using the hoop-strain profiles of the tubes  
605 to assess the PHR height, considering an intimate relationship between the lateral expansion of FRP  
606 tube and inside damage sustained by concrete. This means that the concrete cover may damage with  
607 a high probability when the corresponding hoop strain of FRP tube is high at the same position.  
608 Ozbakkaloglu and Idris (2014) suggested the PHR height can be established through a hoop-  
609 distribution of the specimens at its final loading cycle. They assumed that the PHR terminated at a  
610 height where the hoop strain fell below  $1/3^{\text{rd}}$  of the maximum-recorded strain in the cycle.

611 In this study, the PHR formation and propagation of the three types of tested columns, i.e. RC,  
612 confined RC and confined SRC columns, were determined based on a combined method considering  
613 the hoop strain evolution of the FRP-steel tube and the inside cracking formation of the specimens.  
614 The average PHR height of RC column in the current paper was obtained from the measured height  
615 of two sides of the column after the final load cycle. Regarding other confined RC/SRC columns, the  
616 PHR height of steel tube confined RC/SRC columns (G0S1T0 and G0S1T1) was determined by  
617 analysing the hoop-strain distribution of steel tubes along their height. For the FRP-steel confined  
618 RC/SRC columns, the experimental observation, and strain analyses were conducted to assess their  
619 PHR heights. The results presented in Figs. 5 and 7 show that the difference between the unconfined  
620 and confined columns is high which can be mainly attributed to the different lateral confinement  
621 conditions of the columns. The lateral confinement increases the ductility and deformability of the  
622 columns meaning their PHR heights reduce. In addition, the strain evolutions of the steel tube  
623 confined specimens and FRP-steel confined specimen such as G7S1T0 also show the difference of  
624 the deformation capacity of the region is between 70 mm and 220 mm from the end of the columns.  
625 The additional confinement from the FRP material increases the deformability of the confined  
626 RC/SRC columns. The PHR height of the specimen G7S1T0 should be between 70 mm to 220 mm,  
627 but it is more near to 70 mm. The damage shown in Fig. 5 verifies that the PHR height of the column  
628 G7S1T0 is about 100 mm. Comparing with the specimens G7S1T0 and C7S1T0, the higher elastic  
629 modulus and tensile strength of CFRP increases the hoop strain level at 220 mm from the end of the  
630 columns. However, the hoop strains of the CFRP-steel tube at 70 mm and 220 mm both are quite

631 small, which means its PHR height was not changed significantly being equal to that of GFRP-steel  
632 confined RC columns. It can also be explained by the fact that CFRP and GFRP both are very strong  
633 in tension compared with the steel tube. Within the SRC columns, there was no obvious difference  
634 between the PHR height of steel tube confined SRC columns and FRP-steel confined SRC columns,  
635 which both were about between 70 mm to 100 mm. As described previously, the H-section steel  
636 already makes the RC columns be strong for the resistance of seismic action. This indicates that the  
637 additional lateral confinement of FRP materials does not affect the deformability and ductility of the  
638 columns.

## 639 **6.2 Peak drift level of confined RC columns**

640 As described previously, comparing with conventional RC columns, all confined RC columns of this  
641 study presented an excellent seismic behaviour. However, the lateral load of the columns also started  
642 to cause a degradation with an increase of the lateral displacement after reaching their peak load.  
643 There were many researchers who had explained the reasons of the degradation (e.g. Ang 1985, Cai  
644 et al. 2015) and indicated the degradation of RC columns with increasing lateral displacement was  
645 very important considering safety aspects of the structures subjected to strong earthquake. To promote  
646 the performance- or drift-based design of RC structures subjected to strong earthquake attacks, Cai et  
647 al. (2015) proposed a complete shear design model for circular concrete columns, which was able to  
648 predict the degradation of the lateral shear resistance of the columns under a mega-earthquake. As  
649 shown in their model, Cai et al. (2015) pointed out that the effective lateral confinement factor ( $I_c$ ) of  
650 circular RC columns had a significant influence on the peak drift ratio of the columns, which was  
651 denominated as the degradation-starting drift ratio  $R_{iu}$ . The drift ratio is calculated by a ratio of  $\Delta_{max}/L$   
652 (where,  $\Delta_{max}$  is the displacement corresponding to peak load point and  $L$  is the shear span of the  
653 columns). For discussing the drift ratio of the confined RC columns, this study collected several RC  
654 columns confined by steel tube or FRP-steel tube by existing literature (Liu et al. 2009, Zhou and Liu  
655 2010, Gan et al. 2011, Lin 2012). Using the FEM analysis results in this paper, a data set of the  
656 confined RC columns with shear span ratio ( $a/D$ ) larger than 1.5 and axial load ratio ( $n$ ) exceeding of

657 0.3 was modelled and analysed. In theory, these columns have a stronger trend to fail as flexural  
 658 failure mode. Referring to the model developed by Cai et al. (2015), the effective lateral confinement  
 659 factor ( $I_c$ ) of FRP-steel confined RC columns is calculated by

$$660 \quad I_c = \frac{\rho_{hs} \cdot f_{hs}}{f_{co}} + \frac{\rho_{hst} \cdot f_{hst}}{f_{co}} + \frac{\rho_{hfrp} \cdot f_{hfrp}}{f_{co}} \quad (10)$$

661 where  $\rho_{hs}$  is the volume ratio of stirrup;  $\rho_{hst}$  and  $\rho_{hfrp}$  is the equivalent stirrup volume ratio of the  
 662 steel tube and the FRP tube, respectively;  $f_{hs}$  and  $f_{hst}$  are the yield strength of the stirrup and the  
 663 steel tube, respectively;  $f_{hfrp}$  is the hoop stress of the FRP tube at peak point taken as about 10% of  
 664 ultimate strength of FRP according to the test results;

665

666 Fig.23 shows the relationship between peak drift ratio  $R_{iu}$  and the effective lateral confinement factor  
 667  $I_c$  of the columns confined by the steel or FRP-steel tube, by steel tube and by FRP-steel tube. Results  
 668 show that the factor  $I_c$  has a different influence on the peak drift level of circular confined RC columns  
 669 comparing with the case in circular RC columns. According to existing design codes, most of circular  
 670 RC columns have an  $I_c$  factor less than 0.3 and have a peak drift varying from 0.5% to 2.5%. The  
 671 increasing of  $I_c$  brings a larger increase in the peak drift ratio in Cai et al. model (Cai et al. 2015).  
 672 This can be explained by the fact that the increase of lateral confinement of RC columns has a more  
 673 significant effect on the enhancement of peak drift ratio of shear-dominant columns. In the data  
 674 established in the paper, however, all confined columns are flexural-dominant columns. Besides, the  
 675  $I_c$  factors of the RC columns confined by steel or FRP-steel tube had a larger varying region. The  
 676 peak drifts ratios of the columns increased with the  $I_c$  factors. Comparing with the case of steel tube  
 677 or FRP-steel tube confined RC columns, a stronger linear relationship was found between the  $I_c$  factor  
 678 and the peak drift ratio  $R_{iu}$  of steel tube confined RC columns. However, as shown in Fig.23, the  
 679 existing data of FRP-steel tube confined columns is not enough for determining the relationship  
 680 between  $I_c$  and  $R_{iu}$  in these columns. Therefore, the paper suggests that peak drift ratio  $R_{iu}$  of the RC  
 681 columns confined by steel tube or FRP-steel tube can be calculated simply at the beginning by

$$682 \quad R_{iu} = 2.6I_c + 0.8 \quad (\text{in } \%) \quad (11)$$

## 683 **7. Concluding Remarks**

684 This paper investigated the behaviour of FRP-steel confined concrete columns under reversed cyclic  
685 lateral loads through a series of experiments, including RC (reference column), steel tube confined  
686 RC/SRC columns, and FRP-steel confined RC/SRC columns. Flexural failures were observed for all  
687 columns. The following conclusions can be made:

- 688 • With the increase of the number of FRP layers, the structural behaviours (including yield load  
689 and displacement, peak load and displacement, ultimate load and displacement, and ductility  
690 coefficient) of the FRP-steel confined RC/SRC columns have been improved.
- 691 • The load-carrying capacity, ductility and energy dissipation capacity of FRP-steel confined  
692 RC columns were better than those of RC columns and steel tubes confined RC columns.  
693 Moreover, the improvement caused by the lateral confinement increased as the number of  
694 layers of FRP increased. Similar observations occurred in FRP-steel confined SRC columns  
695 when comparing with SRC column or steel tube confined SRC column.
- 696 • FRP wrapping has no significant effect on the initial stiffness of FRP-steel confined RC/SRC  
697 columns. However, with the increase of the lateral displacement and with more layers of FRP  
698 sheet confining, the stiffness degradation of the columns was reduced.

699 Based on the proposed FEM model verified by the test results in the paper, a parametric analysis has  
700 been conducted to analyse main factors on the behaviour of GFRP-steel confined RC columns. The  
701 main observations are as follows:

- 702 • With the increase of the axial load ratio and the shear span ratio, the load-bearing capacity of  
703 steel tube confined and FRP-steel confined RC columns has been improved, while the ductility  
704 of the columns has been significantly reduced.
- 705 • The load-bearing capacity of steel tube and FRP-steel confined RC columns increased as the  
706 thickness of steel tube increased, while the former kind of the columns increased more  
707 significantly. However, the thickness has no significant influence on the ductility of the columns.
- 708 • The increase of the longitudinal reinforcement ratio improved the load-bearing capacity of steel

709 tube and FRP-steel confined RC columns but just has little effect on the ductility of the columns.

710 • The increase of the number of FRP layers enhanced the ultimate load-bearing capacity and

711 ductility of FRP-steel confined RC columns, but the positive effect was weakened after a

712 certain number of FRP layers were applied. It is need more studies to quantify this for the

713 FRP-steel confined RC columns. The change in the height of FRP wrapping has no significant

714 influence on the load-bearing capacity and ductility the columns after the height reaches 1.5

715 times of the column's diameter.

716 On the other hand, this study discussed the influence of main variables on the plastic hinge region

717 (PHR) height and peak drift ratio of the confined RC columns under reversed cyclic loads and

718 presented that the lateral confinement condition has a significant influence on the PHR height and

719 peak drift ratio of the confined RC columns. Based on the existing test data, the paper suggests a

720 simple model to predict the peak drift ratio of the confined RC columns as well.

## 721 **Acknowledgements**

722 This work was supported by the National Key R&D Program of China (Project No.

723 2017YFC0703008), the National Natural Science Foundation of China (Project No.51778102,

724 51708433), the Fundamental Research Funds for the Central Universities (Project No.

725 DUT18LK35)and the Natural Science Foundation of Liaoning Province of China (Project No.

726 20180550763).

## 727 **References**

728 Aboutaha, R. S., and Machado, R. I. (1999). "Seismic resistance of steel-tubed high-strength

729 reinforced-concrete columns." *J. Struct. Eng.*, 125(5), 485-494.

730 Ang, B.G. (1985). "Seismic shear strength of circular bridge piers." *Rep. No. 85-5*, Department of

731 Civil Engineering, University of Canterbury, Christchurch, New Zealand.

732 Bae, S., and Bayrak, O. (2008). "Plastic hinge length of reinforced concrete columns." *ACI Struct.*

733 *J.*, 105(3), 290.

734 Binici, B. (2005). "An analytical model for stress-strain behavior of confined concrete." *Eng.*  
735 *Struct.*, 27(7), 1040-1051.

736 Cai, G., Sun, Y., Takeuchi, T., and Zhang, J. (2015). "Proposal of a complete seismic shear strength  
737 model for circular concrete columns." *Eng. Struct.*, 100, 399-409.

738 Cao, Q., Tao, J., Wu, Z., and Ma, Z. J. (2017). "Behavior of FRP-Steel Confined Concrete Tubular  
739 Columns Made of Expansive Self-Consolidating Concrete under Axial Compression." *J. Compos.*  
740 *Constr.*, 21(5), 04017037.

741 Gan, D., Guo, L., Liu, J., and Zhou, X. (2011). "Seismic behavior and moment strength of tubed  
742 steel reinforced-concrete (SRC) beam-columns." *J. Constr. Steel Res.*, 67(10), 1516-1524.

743 GB 50010-2010. (2015). "Code for design of concrete structures." Ministry of House and Urban-  
744 Rural Development of People's Republic of China, Beijing (in Chinese)

745 GB/T228-2010. (2009). "Tensile test method for the metal materials at room temperature."  
746 Standardization Administration of the People's Republic of China, Beijing 2010. (in Chinese)

747 Han, L. H., Liu, W., and Yang, Y. F. (2008). "Behavior of thin walled steel tube confined concrete  
748 stub columns subjected to axial local compression." *Thin Wall Struct.*, 46(2), 155-164.

749 Han, L. H., Qu, H., Tao, Z., and Wang, Z. F. (2009). "Experimental behaviour of thin-walled steel  
750 tube confined concrete column to RC beam joints under cyclic loading." *Thin Wall Struct.*, 47(8-9),  
751 847-857.

752 Han, L. H., Yao, G. H., Chen, Z. B., and Yu, Q. (2005). "Experimental behaviours of steel tube  
753 confined concrete (STCC) columns." *Steel Compos. Struct.*, 5(6), 459-484.

754 Hu, H. and Seracino, R. (2013). "Analytical model for FRP-and-steel-confined circular concrete  
755 columns in compression." *J. Compos. Constr.*, 18(3), A4013012.

756 Hu, Y. M., Yu, T. and Teng, J. G. (2011). "FRP-Confined Circular Concrete-Filled Thin Steel  
757 Tubes under Axial Compression." *J. Compos. Constr.*, 15(5), 850-860.

758 Huang, P.D. (2016). "Cyclic Axial Compression Mechanical Behavior Study of GFRP-Steel  
759 Composite Tube Confined RC Stub Columns." MS Thesis of Dalian University of Technology,

760 Dalian. [In Chinese]

761 Inel, M., and Ozmen, H. B. (2006). "Effects of plastic hinge properties in nonlinear analysis of  
762 reinforced concrete buildings." *Eng. Struct.*, 28(11), 1494-1502.

763 JGJ3-2002. (2002). "Technical Specification for Concrete Structures of Tall Buildings."  
764 Standardization Administration of the People's Republic of China, Beijing; 2002. (in Chinese)

765 Jiang, T., and Teng, J. G. (2007). "Analysis-oriented models for FRP-confined concrete." *Eng.*  
766 *Struct.*, 29, 2968-2986.

767 Kent, D.C. and Park, R. (1971) "Flexural members with confined concrete." *J. Struct. Division*,  
768 97(7), 1969-1990.

769 Lam, L., and Teng, J.G. (2009). "Stress-strain model for FRP-confined concrete under cyclic axial  
770 compression". *Eng. Struct.*, 31(2), 308-321.

771 Li, Y. F., Chen, S. H., Chang, K. C., and Liu, K. Y. (2005). "A constitutive model of concrete  
772 confined by steel reinforcements and steel jackets." *Can. J. Civil Eng.*, 32(1), 279-288.

773 Lin, S. L. (2012). "Seismic performance of FRP-steel composite tube confined RC columns." MS  
774 Thesis of Harbin Institute of Technology, Harbin. (In Chinese)

775 Liu, J. P., Xu, T. X., Wang, Y. H., and Guo, Y. (2018). "Axial behaviour of circular steel tubed concrete  
776 stub columns confined by CFRP materials." *Constr. Build Mater.*, 168, 221-231.

777 Liu, J., and Sheikh, S. A. (2013). "Fiber-reinforced polymer-confined circular columns under  
778 simulated seismic loads." *ACI Struct. J.*, 110(6), 941.

779 Liu, J., Zhang, S., Zhang, X., and Guo, L. (2009). "Behavior and strength of circular tube confined  
780 reinforced-concrete (CTRC) columns." *J. Constr. Steel Res.*, 65(7), 1447-1458.

781 Liu, L., and Lu, Y. (2010). "Axial bearing capacity of short FRP confined concrete-filled steel  
782 tubular columns." *J. Wuhan Univ. Tech.-Mater. Sci. Ed.*, 25(3), 454-458.

783 Mazzoni, S., McKenna, F., Scott, M.H., and Fenves, G.L. (2006). *OpenSees command language*  
784 *manual*. Pacific Earthquake Engineering Research (PEER) Center.

785 Menegotto, M., and E. Pinto. (1973). "Method of analysis for cyclically loaded reinforced concrete  
786 plane frames including changes in geometry and non-elastic behavior of elements under combined  
787 normal force and bending." Proc., IABSE Symposium. Lisbon, Portugal, 15-22.

788 Orakcal, K., Massone, L.M.,Wallence, J.W. (2006). "Analytical modeling of reinforced concrete  
789 walls for predicting flexural and coupled-shear-flexural responses." PEER, University of California.  
790 USA.

791 Ozbakkaloglu, T., and Idris, Y. (2014). "Seismic behavior of FRP-high-strength concrete–steel  
792 double-skin tubular columns." *J. Struct. Eng.*, 140(6), 04014019.

793 Ozbakkaloglu, T., and Saatcioglu, M. (2006). "Seismic behavior of high-strength concrete columns  
794 confined by fiber-reinforced polymer tubes." *J. Compos. Constr.*, 10(6), 538-549.

795 Ozbakkaloglu, T., and Saatcioglu, M. (2007). "Seismic performance of square high-strength  
796 concrete columns in FRP stay-in-place formwork." *J. Struct. Eng.*, 133(1), 44-56.

797 Park, J. W. and Choi, S. M. (2013). "Structural behavior of CFRP strengthened concrete-filled  
798 steel tubes columns under axial compression loads". *Steel Compos. Struct.*, 14(5), 453-472.

799 Park, J. W., Hong, Y. K. and Choi, S. M. (2010). "Behaviors of concrete filled square steel tubes  
800 confined by carbon fiber sheets (CFS) under compression and cyclic loads." *Steel Compos.*  
801 *Struct.*, 10(2), 187-205.

802 Park, R. (1988). "State of the art report ductility evaluation from laboratory and analytical testing."  
803 Proc., 9th World Conf. Earthq. Eng., Tokyo, Kyoto, Japan, 605-616.

804 Popovics, S. (1973). "A numerical approach to the complete stress-strain curve of  
805 concrete." *Cement Concrete Res.*, 3(5), 583-599.

806 Ran J.H. (2014). "Axial Compression Mechanical Behavior of FRP-Steel Composite Tube  
807 Confined Concrete Stub Columns." MS Thesis of Dalian University of Technology, Dalian. [In  
808 Chinese]

809 Sakino, K., Nakahara, H., Morino, S., and Nishiyama, I. (2004). Behavior of centrally loaded  
810 concrete-filled steel-tube short columns. *J. Struct. Eng.*, 130(2), 180-188

811 Scott, B. D., Park, R., and Priestley, M. J. N. (1982). "Stress-strain behavior of concrete confined  
812 by overlapping hoops at low and high strain rates." *ACI Struct. J.*, 79(1), 13-27.

813 Tao, Z., Wang, Z., Han, L. and Uy, B. (2011). "Fire performance of concrete-filled steel tubular  
814 columns strengthened by CFRP." *Steel Compos. Struct.*, 11(4), 307-324.

815 Teng, J. G., Hu, Y. M. and Yu, T. (2013). "Stress-strain model for concrete in FRP-confined steel  
816 tubular columns." *Eng. Struct.*, 49(2),156-167.

817 Tomii, M., Sakino, K., Watanabe, K. and Xiao, Y. (1985a). "Lateral load capacity of reinforced  
818 concrete short columns confined by steel tube", *Proc., Int'l Speciality Conf. Concr. Filled Steel*  
819 *Tubular Struct.*, Harbin, China, August, pp. 19-26.

820 Tomii, M., Sakino, K., Xiao, Y. and Watanabe, K. (1985b). "Earthquake resisting hysteretic  
821 behavior of reinforced concrete short columns confined by steel tube", *Proc., Int'l Speciality Conf.*  
822 *Concr. Filled Steel Tubular Struct.*, Harbin, China, August, pp. 119-125.

823 Wang, D.Y. (2012). "Experimental and analytical investigation of seismic performance of nonductile  
824 RC frames retrofitted with FRP." *Ph.D Dissertation of Harbin Institute of Technology*, Harbin. (in  
825 Chinese)

826 Wang, Z., Yu, Q. and Tao, Z. (2015). "Behaviour of CFRP externally-reinforced circular CFT  
827 members under combined tension and bending." *J. Constr. Steel Res.*, 106, 122-137.

828 Wu, Z., Wang, X., Zhao, X., and Noori, M. (2014). "State-of-the-art review of FRP composites for  
829 major construction with high performance and longevity." *J. Sustainable Mater. Struct. Sys.*, 1(3),  
830 201-231.

831 Xiao, Y. (2004). "Applications of FRP composites in concrete columns." *Adv. Struct. Eng.*, 7(4),  
832 335-343.

833 Xiao, Y., He, W., and Choi, K. K. (2005). "Confined concrete-filled tubular columns." *J. Struct.*  
834 *Eng.*, 131(3), 488-497.

835 Youssf, O., ElGawady, M. A., and Mills, J. E. (2015). "Displacement and plastic hinge length of  
836 FRP-confined circular reinforced concrete columns." *Eng. Struct.*, 101, 465-476.

837 Yu, Q., Tao, Z., Liu, W., and Chen, Z. B. (2010). "Analysis and calculations of steel tube confined  
838 concrete (STCC) stub columns." *J. Constr. Steel Res.*, 66(1), 53-64.

839 Yu, T., Hu, Y. M. and Teng J. G. (2016). "Cyclic lateral response of FRP-confined circular  
840 concrete-filled steel tubular columns." *J. Constr. Steel Res.*, 124, 12-22.

841 Yuan, F., Wu, Y. F., and Li, C. Q. (2017). "Modelling plastic hinge of FRP-confined RC  
842 columns." *Eng. Struct.*, 131, 651-668.

843 Zhou, X. H., Liu, J. P., Wang, X., and Chen, Y. F. (2016). "Behavior and design of slender circular  
844 tubed-reinforced-concrete columns subjected to eccentric compression." *Eng. Struct.*, 124, 17-28.

845 Zhou, X. H., Yan, B., and Liu, J. P. (2015). "Behavior of square tubed steel reinforced-concrete  
846 (SRC) columns under eccentric compression." *Thin Wall Struct.*, 91, 129-138.

847 Zhou, X., Cheng, G., Liu, J., Gan, D., and Chen, Y. F. (2017). "Behavior of circular tubed-RC  
848 column to RC beam connections under axial compression." *J. Constr. Steel Res.*, 130, 96-108.

849 Zhou, X.H., and Liu, J. P. (2010). "Seismic behavior and shear strength of tubed RC short  
850 columns." *J. Constr. Steel Res.*, 66(3), 385-397.

1 **Tables**

2 Table 1 Details of test specimens

3 Table 2 Material properties of steel, FRP and epoxy adhesive

4 Table 3 Summary of the test results of test specimens

5

6

7

Table 1 Details of test specimens

Test No.	Diameter D /mm	Thickness $t_s$ /mm	Reinforcing bars	Stirrups	The number of layers of FRP sheet	FRP type	Setting of H-Steel
G0S0T0	300	-			-	-	No
G0S1T0	300	3			-	-	No
G5S1T0	300	3			5	GFRP	No
G7S1T0	300	3	6 $\Phi$ 16	$\Phi$ 8@100	7	GFRP	No
C7S1T0	300	3			7	CFRP	No
G0S1T1	300	3			-	-	Yes
G5S1T1	300	3			5	GFRP	Yes
G7S1T1	300	3			7	GFRP	Yes

Noted: G/Cx: x-layers GFRP or CFRP sheet; S0/S1: without/with confined steel tube; T0/T1: without/with H-steel;

8

9

Table 2 Material properties of steel, FRP and epoxy adhesive

Materials	Diameter or thickness (mm)	Young's modulus $E_s$ /GPa	Yielding strength $f_y$ /MPa	Tensile strength $f_u$ /MPa
Steel tube Q235	3	210	280	414
Stirrups Q345	8	206	400	540
Reinforcing rebar Q345	16	205	420	590
H-Steel wing/web plates	10/7	208/221	223/225	374/387

Materials	Thickness $t_{fp}$ /mm	Young's modulus E /GPa	Elongation $\delta$ /%	Tensile strength f /MPa
CFRP	0.167	245	1.51	4077
GFRP	0.354	72	2.1	1500
Epoxy	-	$\geq 2.4$	$\geq 1.50$	$\geq 38$

10

11

12

Table 3 Summary of the test results of test specimens

Specimens	$P_y$	$\Delta_y$ /mm	$P_{max}$ /kN	$\Delta_{max}$ /mm	$P_u$ /kN	$\Delta_u$ /mm	R/%	$\mu_\Delta$
G0S0T0	80.55	8.30	92.95	13.42	79.01	16.44	1.37	1.98
G0S1T0	96.44	10.49	110.95	21.68	94.30	43.90	3.66	4.19
G5S1T0	101.84	12.37	122.29	24.91	103.95	52.11	4.34	4.21
G7S1T0	107.01	14.53	128.72	27.83	109.41	62.70	5.23	4.32
C7S1T0	103.81	11.52	122.97	24.60	104.53	51.37	4.28	4.46
G0S1T1	149.83	13.99	158.45	35.79	134.68	72.64	6.05	5.19
G5S1T1	150.34	14.78	172.46	36.22	155.22	77.81	6.48	5.26
G7S1T1	165.07	15.47	186.78	39.75	168.10	81.99	6.83	5.30

Noted:  $\mu_\Delta$  is displacement ductility coefficient, which is calculated by  $\Delta_u/\Delta_y$ .

13

Fig.1

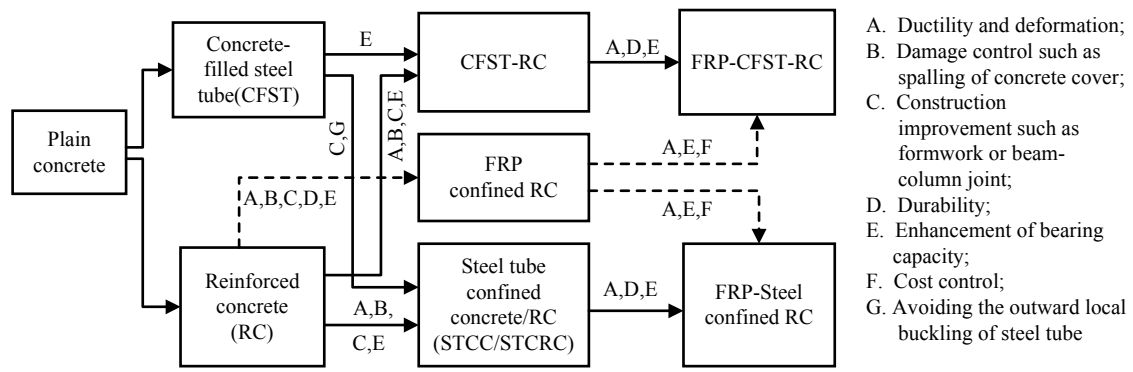


Fig.1 Development of reinforced concrete and confined concrete in past decades

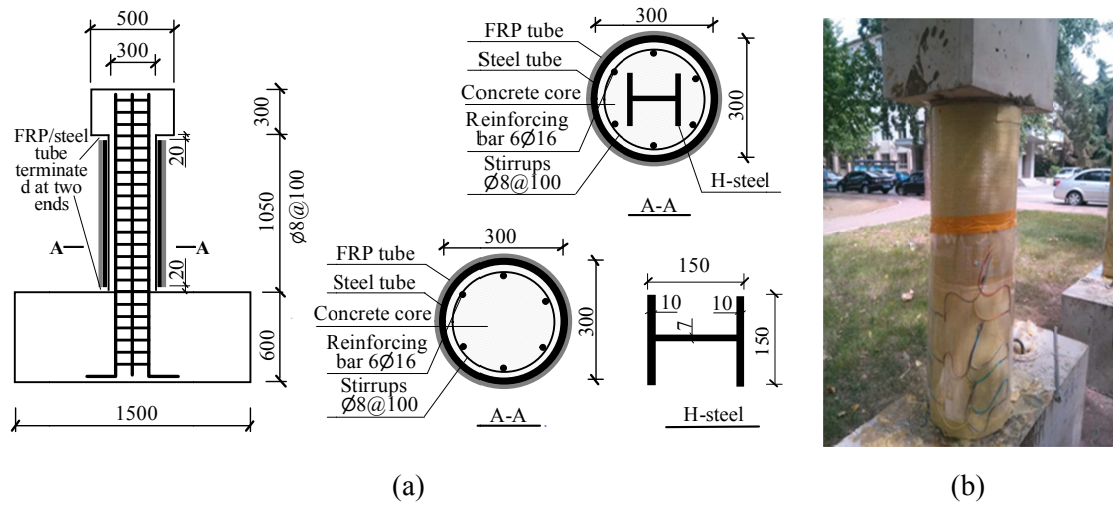


Fig. 2 Details of test specimens (Units in mm): (a) Dimension and reinforcement arrangement; (b) Confined columns

Fig.3

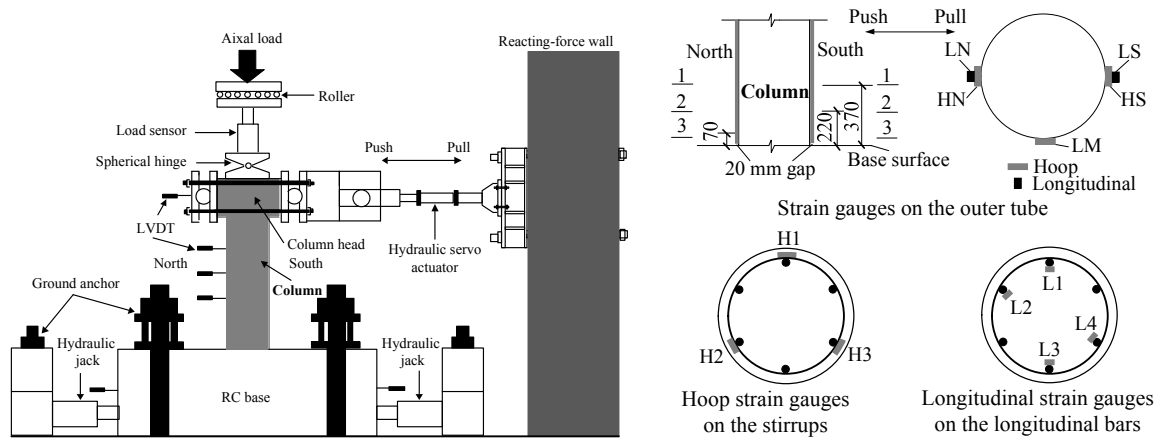


Fig. 3 Test setup and layout of LVDTs and strain gauge (Units in mm)

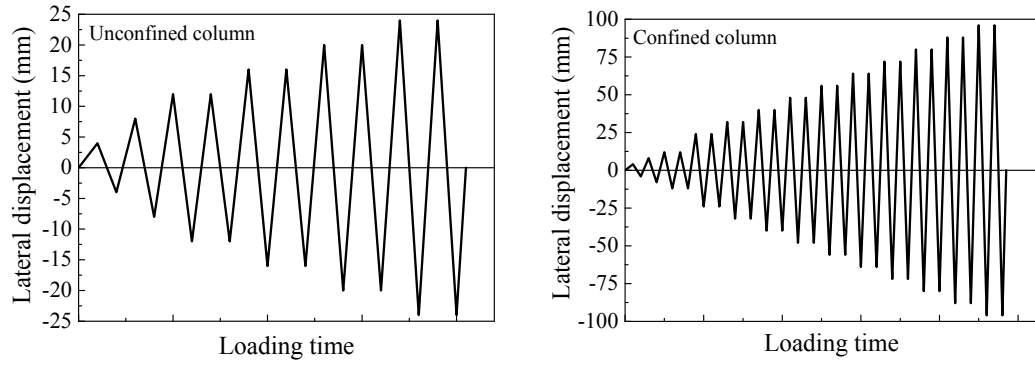


Fig. 4 Loading procedure

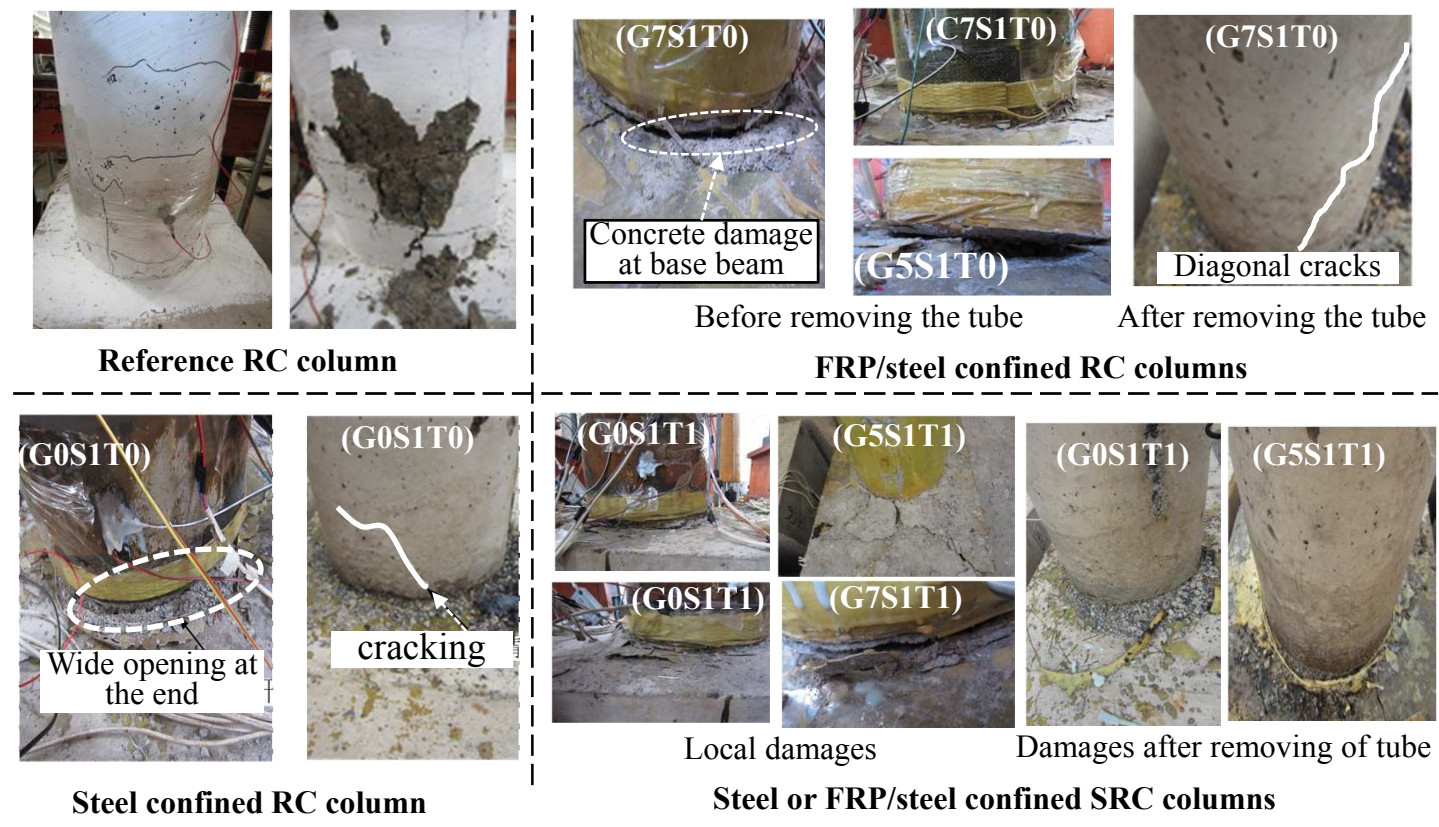


Fig. 5 Damages and cracks of the specimens

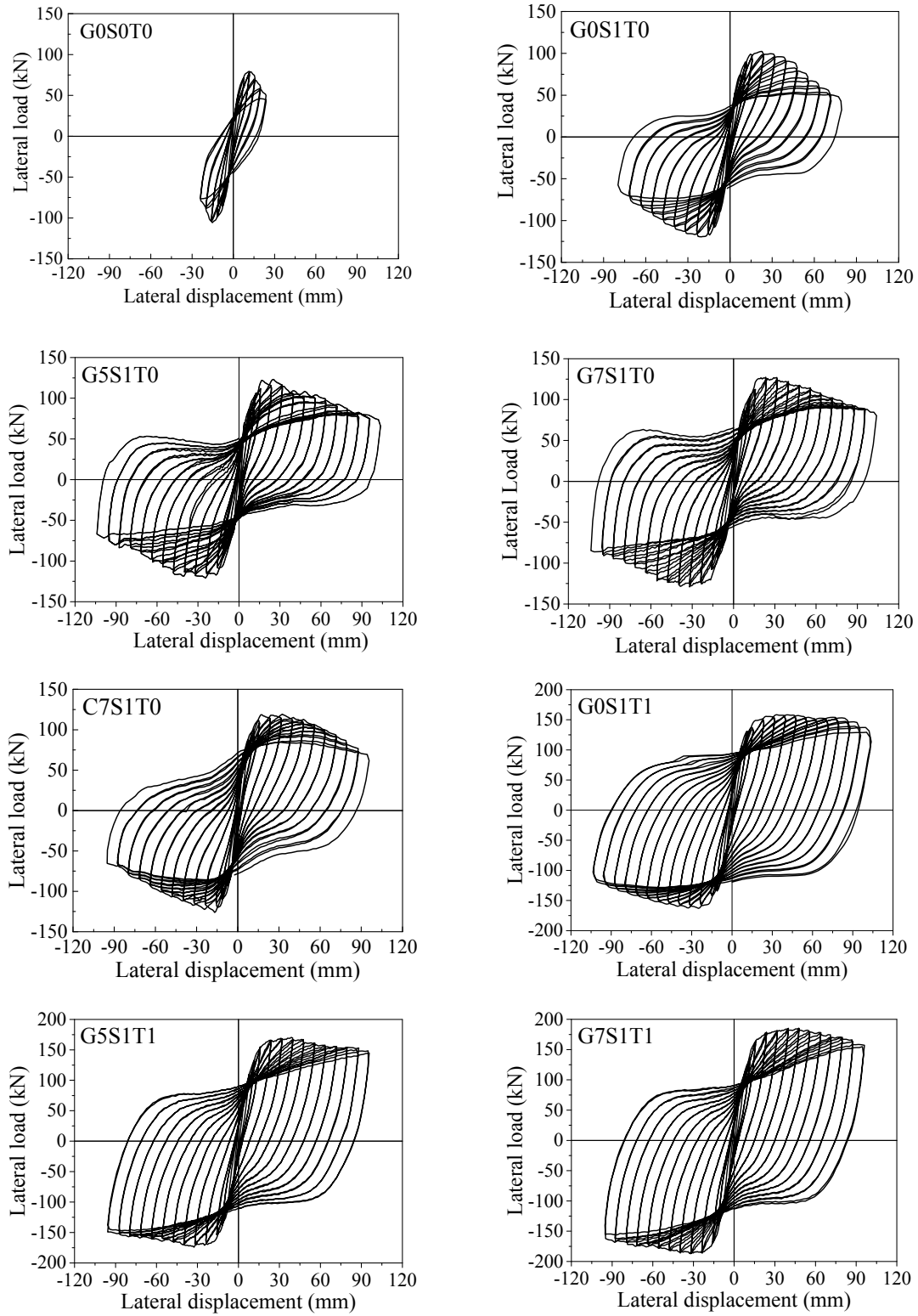


Fig.6 Hysteresis behavior of the specimens

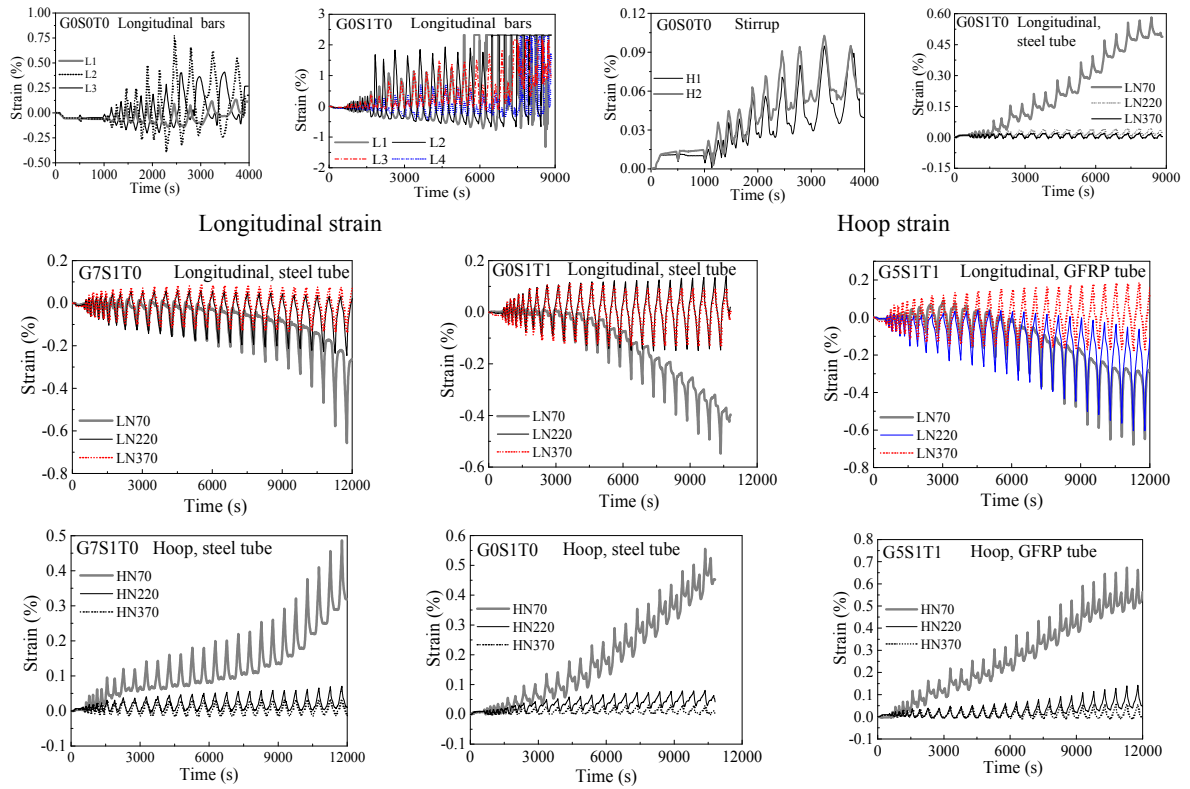


Fig. 7 Strain evolution of reinforcing bars, steel tube and FRP tube

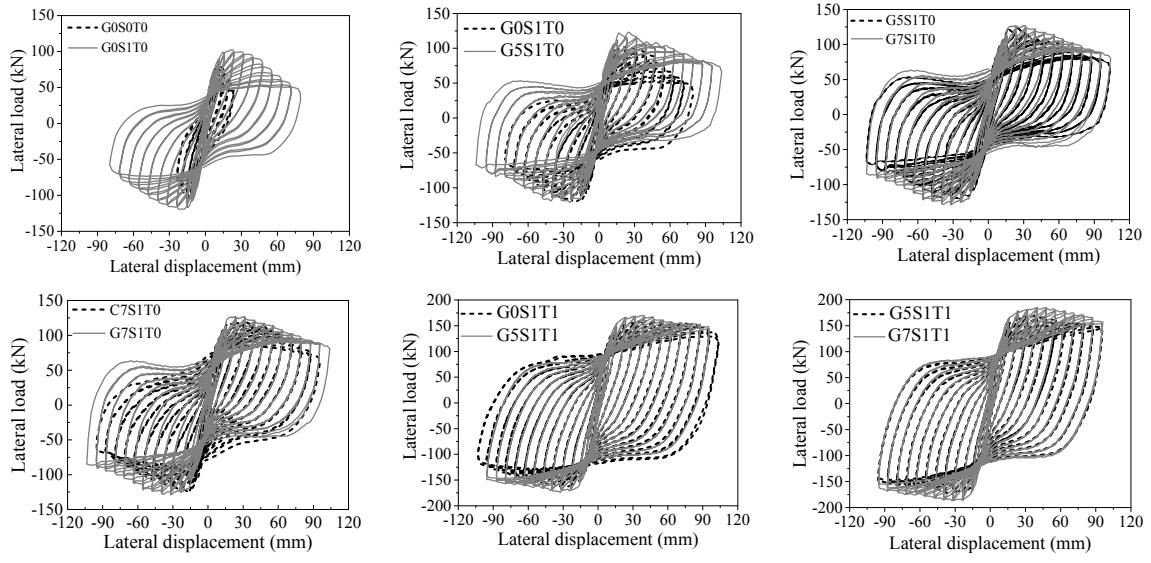


Fig. 8 Comparison of experimental lateral load-displacement curves

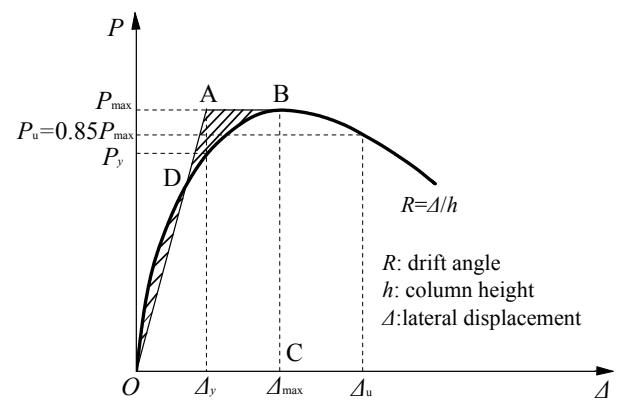


Fig. 9 Ductility calculation method – the equivalent elastoplastic energy absorption method (Park 1988)

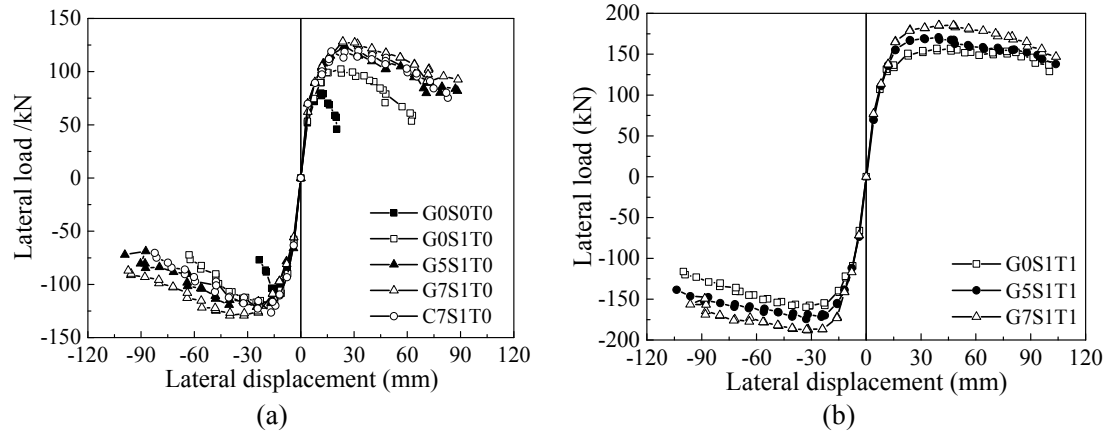


Fig. 10 Experimental load-displacement skeleton curves: (a) Without H-steel; (b) With H-steel

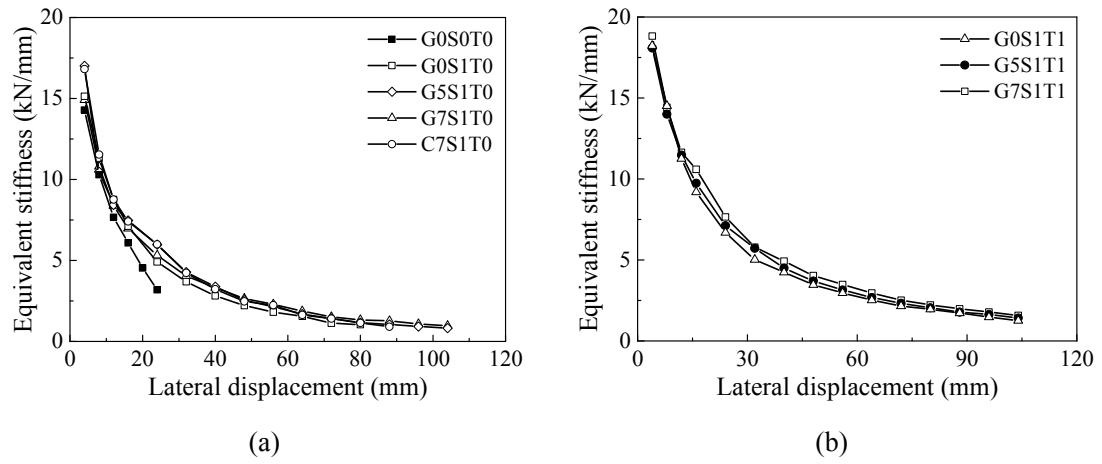


Fig. 11 Evolution of the equivalent stiffness of test specimens: (a) Without H-steel; (b) With H-steel

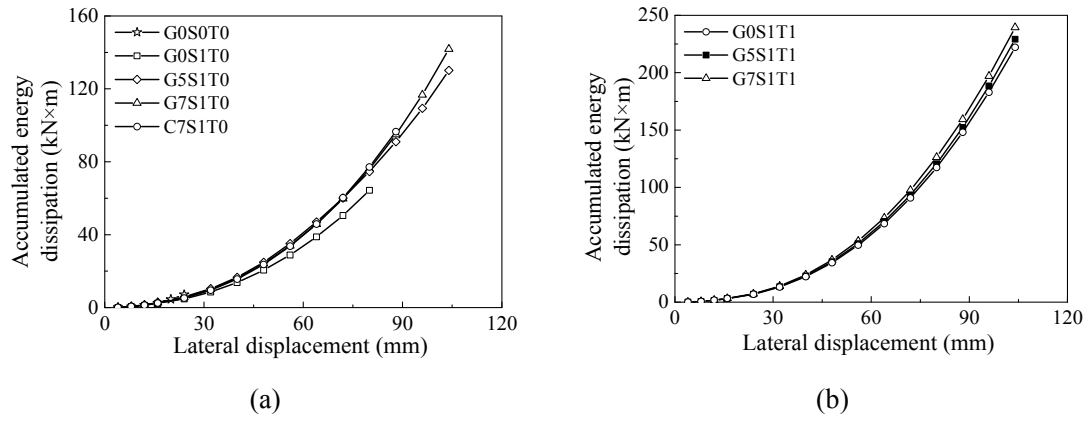


Fig. 12 Accumulated energy dissipation of the test specimens: (a) Without H-steel; (b) With H-steel

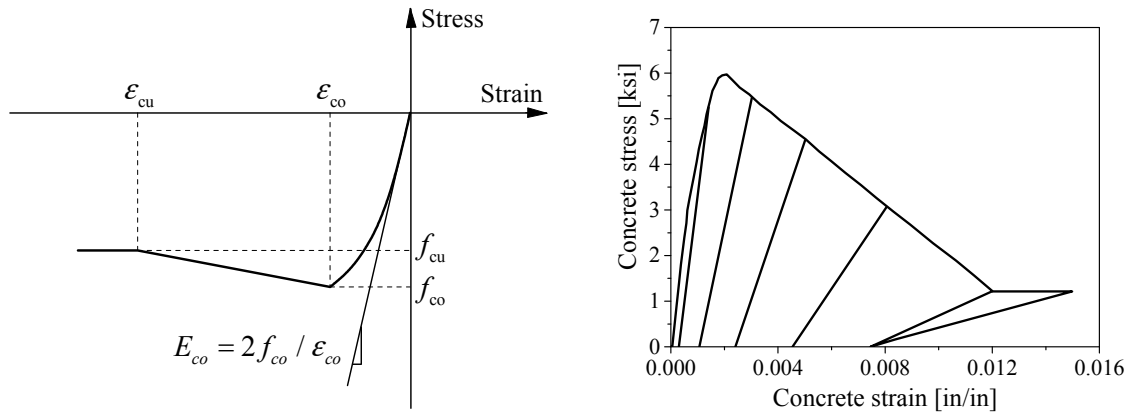


Fig. 13 Stress-strain models of Concrete01 in OpenSees (Mazzoni et al. 2006)

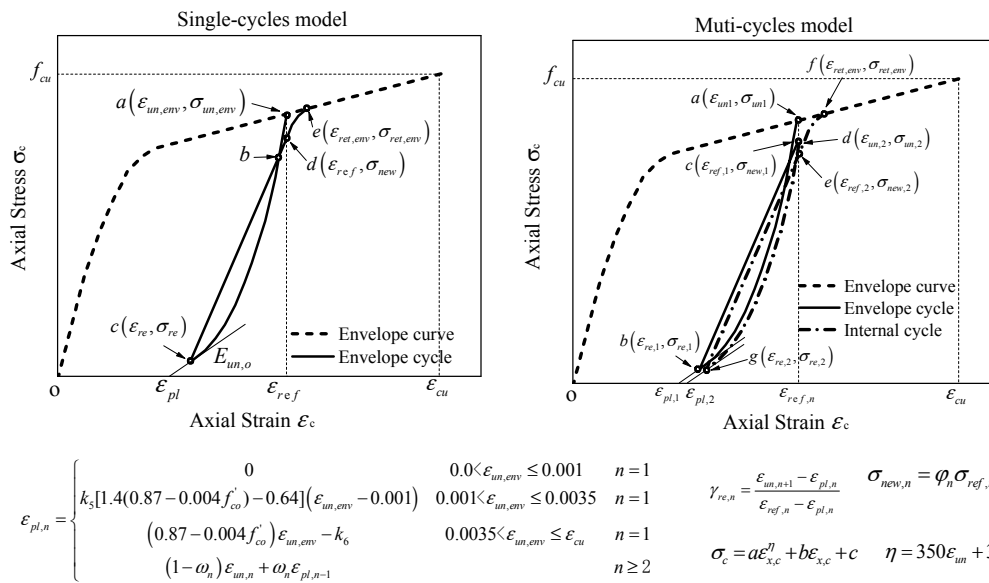


Fig. 14 Key parameters of proposed cyclic constitutive models (Huang 2016)

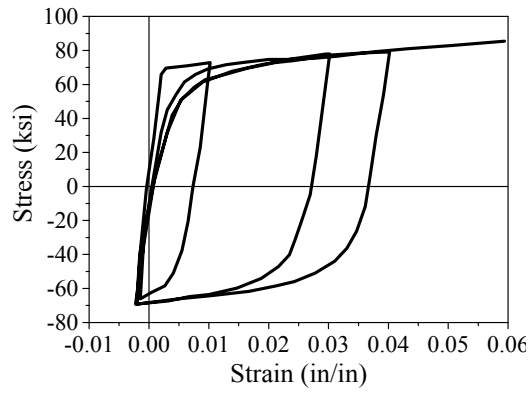


Fig. 15 Hysteretic property of Steel02 model in OpenSees

Fig.16

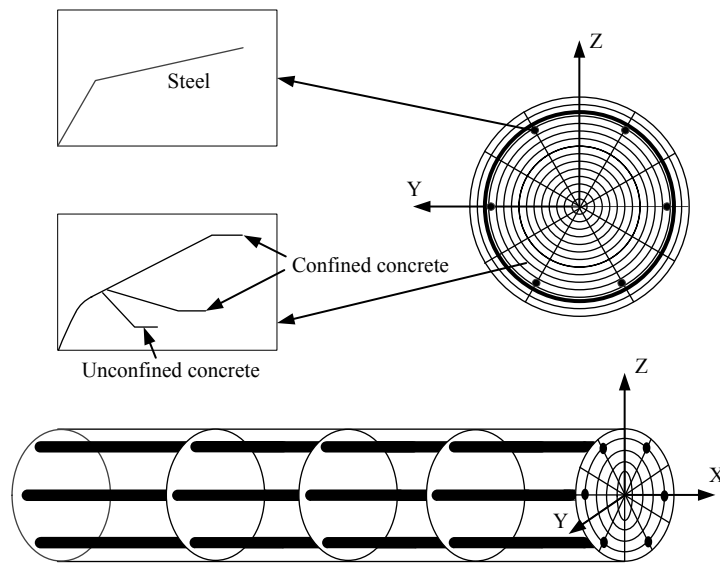


Fig. 16 Schematic representation of the fibre's cross-section

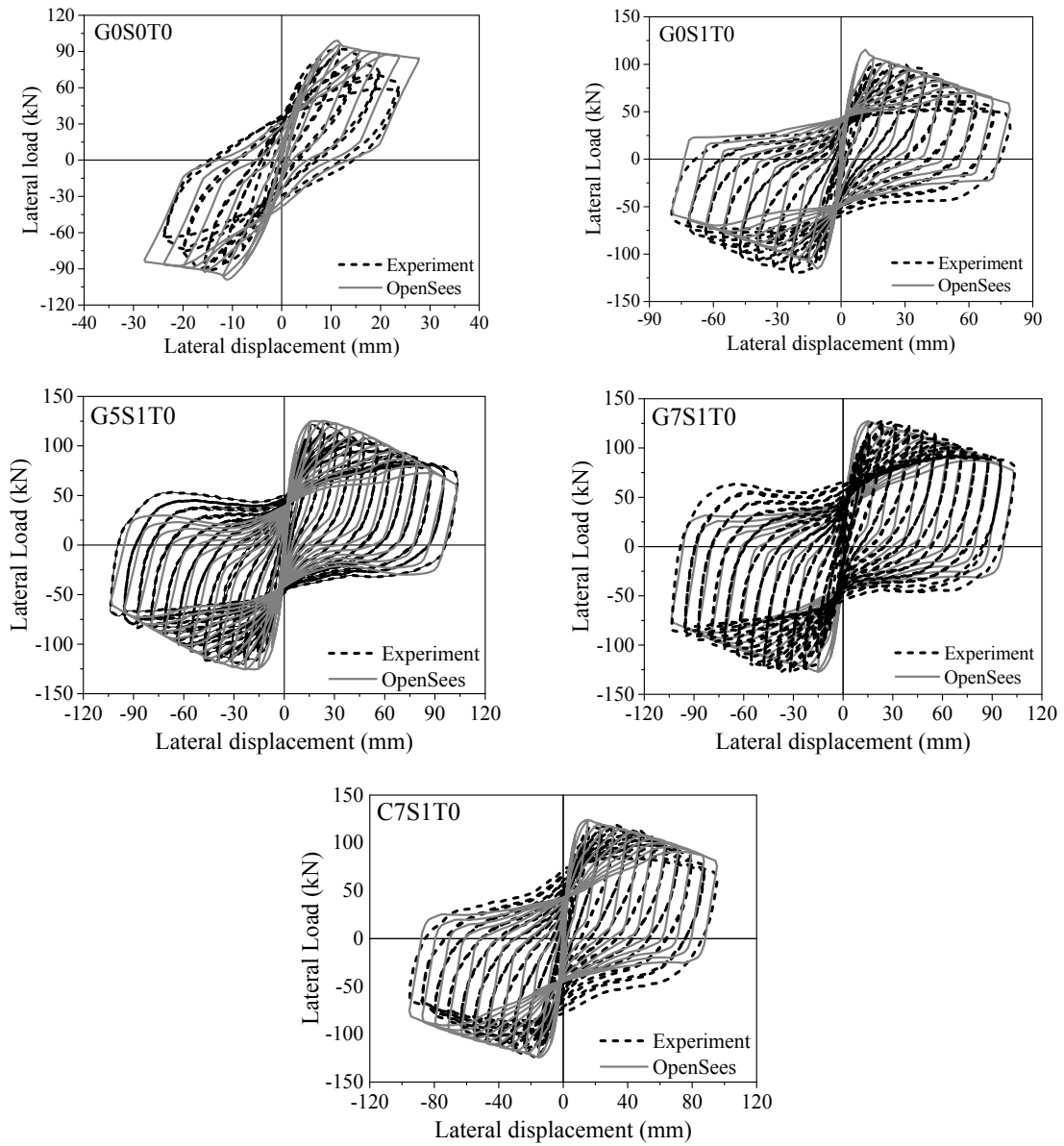


Fig. 17 Comparison between simulation and test results of circular RC and confined RC columns

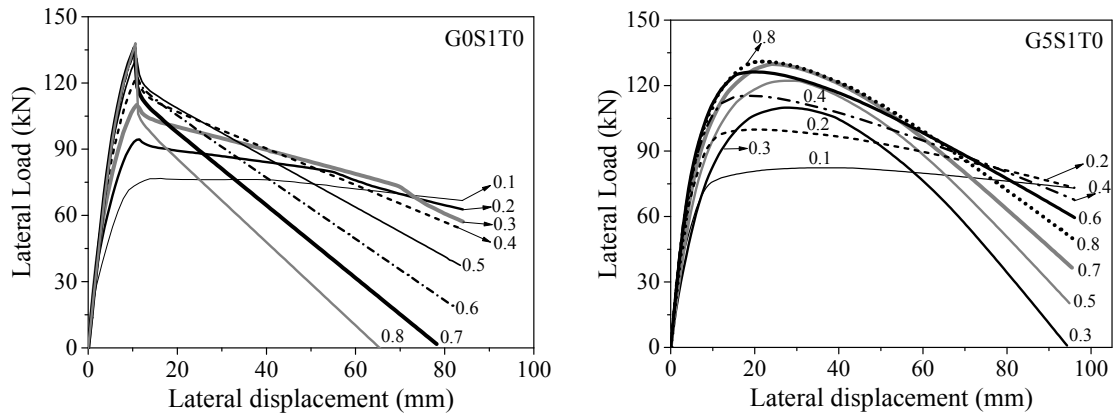


Fig. 18 Influence of axial load ratio on FRP-steel confined RC columns

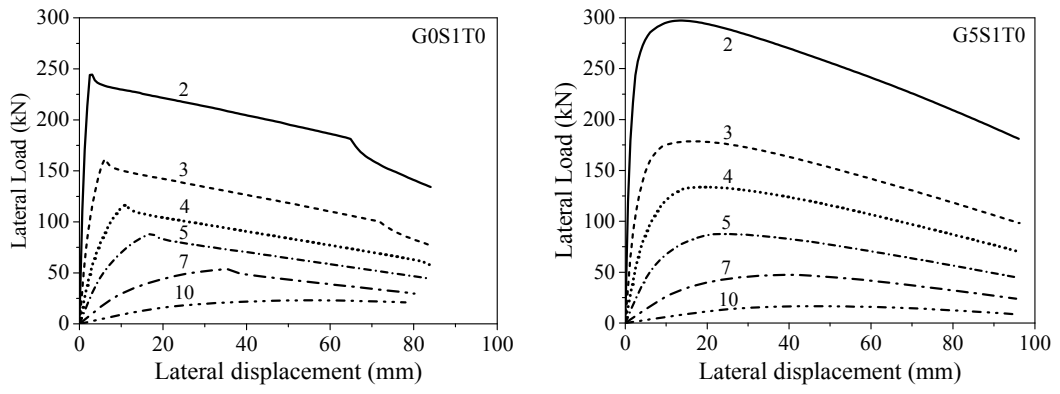


Fig. 19 Influence of shear-span ratio on FRP-steel confined RC columns

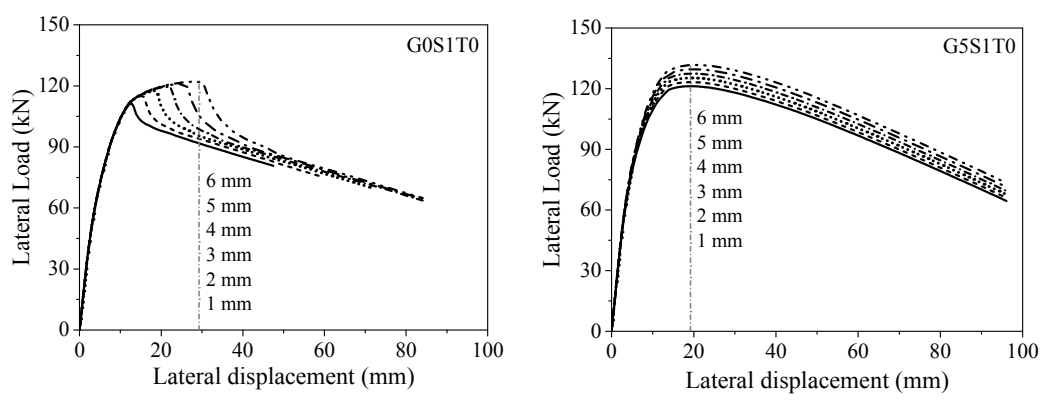


Fig. 20 Effects of steel tube thickness on FRP-steel confined RC columns

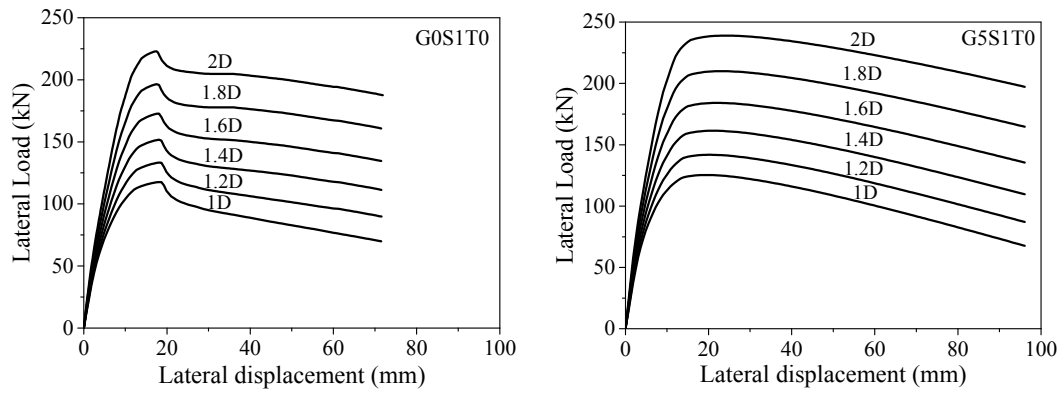


Fig. 21 Effects of longitudinal bars ratio on FRP-steel confined RC columns

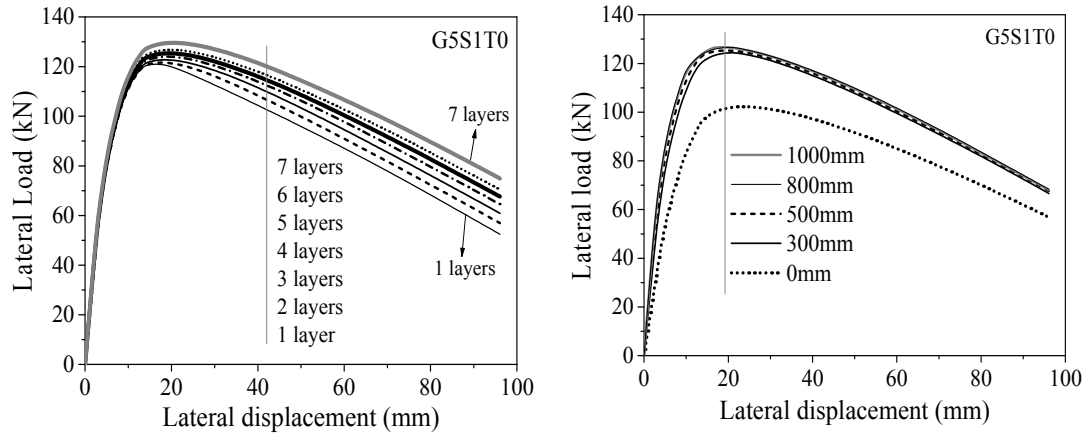


Fig. 22 Effects of confining layer number and the height of GFRP on the confined columns

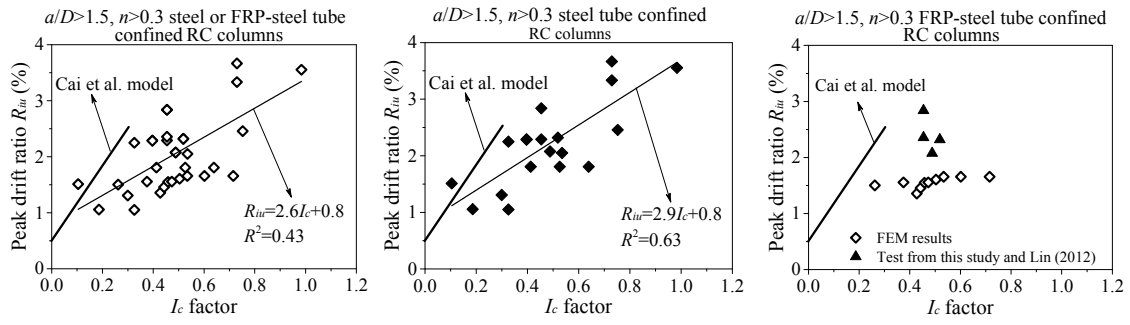


Fig.23 Relationship between peak drift ratio and  $I_c$  factor of confined RC columns